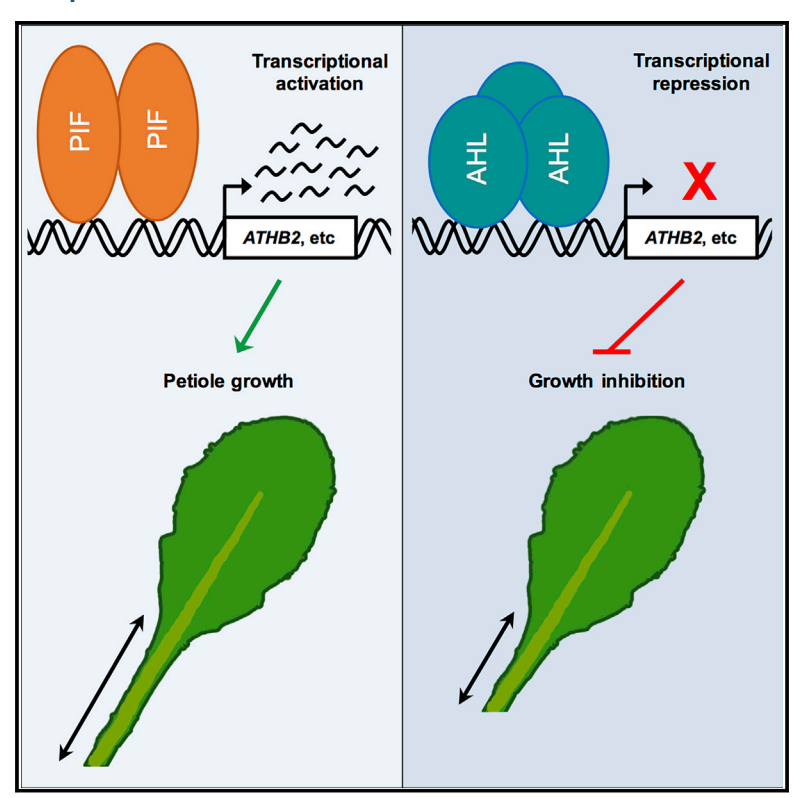
Current Biology

AT-Hook Transcription Factors Restrict Petiole Growth by Antagonizing PIFs

Graphical Abstract



Authors

David S. Favero, Ayako Kawamura, Michitaro Shibata, ..., Philip A. Wigge, Michael M. Neff, Keiko Sugimoto

Correspondence

david.favero@riken.jp

In Brief

Favero et al. demonstrate that the AHL transcription factors repress leaf petiole elongation by antagonizing key regulators of plant growth, the PIFs. AHLs bind to PIF-targeted loci and reduce PIF binding to these regions, thus inhibiting transcriptional activation of growth-promoting genes.

Highlights

- AHL transcription factors repress petiole elongation in juvenile rosettes
- The effect of AHLs on petiole growth is dependent on PIFs
- AHLs bind to and repress the expression of genes directly activated by PIFs
- PIF binding to target genes is reduced by ectopic AHL expression





AT-Hook Transcription Factors Restrict Petiole Growth by Antagonizing PIFs

David S. Favero,^{1,6,7,10,*} Ayako Kawamura,¹ Michitaro Shibata,¹ Arika Takebayashi,¹ Jae-Hoon Jung,^{2,3} Takamasa Suzuki,⁴ Katja E. Jaeger,^{2,5} Takashi Ishida,^{1,9} Akira Iwase,¹ Philip A. Wigge,^{2,5} Michael M. Neff,^{6,7} and Keiko Sugimoto^{1,8}

SUMMARY

Upon detecting abiotic or biotic stress, plants generally reduce their growth, enabling resources to be conserved and diverted to stress response mechanisms. In Arabidopsis thaliana, the AT-hook motif nuclear-localized (AHL) transcription factor family has been implicated in restricting rosette growth in response to stress. However, the mechanism by which AHLs repress growth in rosettes is unknown. In this study, we establish that SUPPRESSOR OF PHYTOCHROME B4-#3 (SOB3) and other AHLs restrict petiole elongation by antagonizing the growth-promoting PHYTOCHROME-INTERACTING FACTORs (PIFs). Our data show that high levels of SOB3 expression lead to a short-petiole phenotype similar to that conferred by removal of PIF4. Conversely, the dominant-negative sob3-6 mutant has long petioles, a phenotype which is PIF-dependent. We further show that AHLs repress the expression of many PIF-activated genes, several of which are involved in hormone-mediated promotion of growth. Additionally, a subset of PIF-activated, AHL-repressed genes are directly bound by both SOB3 and PIFs. Finally, SOB3 reduces binding of PIF4 to shared target loci. Collectively, our results demonstrate that AHLs repress petiole growth by antagonizing PIF-mediated transcriptional activation of genes associated with growth and hormone pathways. By elucidating a mechanism via which the stress-responsive AHL transcription factor family influences growth in petioles, this study identifies a key step in the gene regulatory network controlling leaf growth in response to the environment.

INTRODUCTION

As sessile organisms, plants rely heavily on growth and developmental plasticity to respond to external challenges threatening their survival. A complex network of hormone and other signaling pathways enables plants to respond appropriately to a wide variety of different types of stress, including low nutrient levels, drought, excess light, and pathogen attack [1, 2]. Many types of stress provoke a reduction in plant growth, which enables the conservation of resources that may be scarce or needed for mounting a defense response. Such tradeoffs between growth and defense in plants are regulated by transcription factors like the PHYTOCHROME-INTERACTING FACTORs (PIFs), which function as key positive regulators of growth and are also associated with gene regulatory networks that coordinate plant responses to the environment [3–7].

Work over the past few years, mainly in *Arabidopsis thaliana* (*Arabidopsis*), has implicated the AT-hook motif nuclear localized (AHL) family in both stress responses and regulation of growth and development. AHLs are transcription factors, found specifically in land plants, that are characterized by the presence of two conserved regions: a plant and prokaryote conserved (PPC) domain, involved in protein-protein interactions, and one or two DNA-binding AT-hook motif(s) [8–10]. Although the mechanism(s) by which AHLs regulate transcription are not well established, findings from several studies suggest that they may affect target gene expression by recruiting chromatin modifiers [11–15]. *AHL*s affect hypocotyl growth [9, 15–19], floral transition [12, 13, 19, 20], inflorescence and flower development [21–25], senescence [11], vascular tissue patterning [26], and immunity [27, 28], and their transcription is known to be activated by a



¹RIKEN Center for Sustainable Resource Science, Yokohama, Kanagawa 230-0045, Japan

²Sainsbury Laboratory, University of Cambridge, Cambridge CB2 1LR, UK

³Department of Biological Sciences, Sungkyunkwan University, Suwon 16419, South Korea

⁴Department of Biological Chemistry, College of Biosciences and Biotechnology, Chubu University, Kasugai, Aichi 487-8501, Japan

⁵Leibniz-Institut für Gemüse- und Zierpflanzenbau (IGZ), Großbeeren 14979 Germany

⁶Department of Crop and Soil Sciences, Washington State University, Pullman, WA 99164 USA

⁷Molecular Plant Sciences Graduate Program, Washington State University, Pullman, WA 99164 USA

⁸Department of Biological Sciences, The University of Tokyo, Tokyo 119-0033, Japan

⁹Present address: International Research Organization for Advanced Science and Technology, Kumamoto University, Kumamoto 860-8555, Japan

¹⁰Lead Contact

^{*}Correspondence: david.favero@riken.jp https://doi.org/10.1016/j.cub.2020.02.017

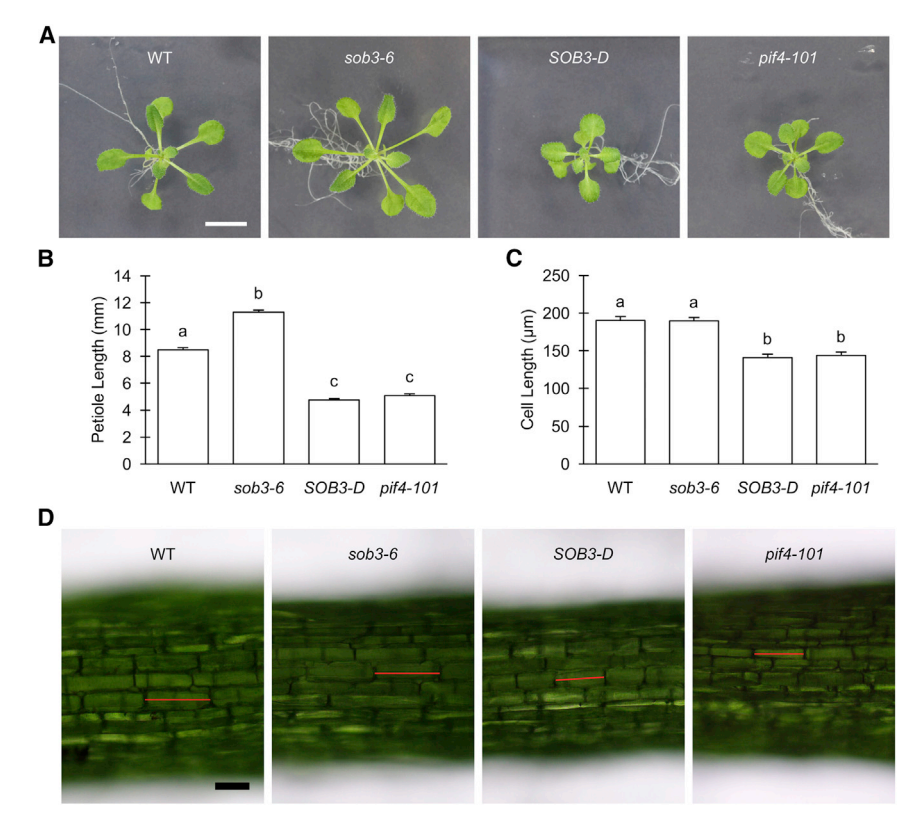


Figure 1. SOB3 Represses Petiole Growth

(A) Representative juvenile rosettes of mutants for SOB3 and PIF4 and the wild-type (WT), Col-0. Scale bar equals 10 mm.

(B and C) Quantification of leaf 4 petiole lengths (B) and lengths of cortex cells in leaf 4 petioles (C) for 21-day-old plants of the genotypes pictured in (A). Bar graph values represent means of measured petiole lengths (B) or cell lengths (C) for each genotype and error bars represent SEM. Different letters indicate significant differences based on one-way ANOVA with Tukey's HSD test (p < 0.001).

(D) Microscopic images of representative cortex cells viewed from the abaxial side of leaf 4 petioles from WT, sob3-6, SOB3-D, and pif4-101. Scale bar, 100 um.

See also Figure S1.

variety of different types of stress [29-31]. Furthermore, a recent study in Arabidopsis found that AHL10 is activated via phosphorylation in response to moderate drought stress, where it restricts rosette biomass accumulation via an unknown mechanism [29].

In this study, we sought to further investigate the effect of AHLs on rosette growth by focusing on the petiole. Our findings indicate that SUPPRESSOR OF PHYTOCHROME B4-#3 (SOB3/ AHL29) and other AHLs repress petiole elongation by inhibiting PIF-mediated transcriptional activation of growth-promoting genes. Specifically, AHLs associate with similar loci as those targeted by PIFs and reduce PIF binding to target genes. This study thus reveals a mechanism by which PIF activity is modulated within the gene regulatory network that regulates leaf growth in response to both internal and external cues.

RESULTS

AHLs Repress Petiole Growth

In order to investigate the effect of AHLs on rosette growth, we examined petiole phenotypes in mutants for SOB3 starting with two previously characterized lines, SOB3-D and sob3-6 [9, 18]. We observed a short-petiole phenotype in SOB3-D, which has high SOB3 expression, while the dominant-negative sob3-6 mutant has increased petiole growth (Figures 1A and 1B). In addition to sob3-6, we also observed enhanced petiole growth in esc-11 (Figure S1A), a dominant-negative mutant for SOB3's closets homolog, ESC (also known as AHL27) [9]. Taken together, these results indicate that AHLs repress petiole growth. We next investigated whether AHLs influence cell expansion or cell division in petioles by measuring the lengths of cortex cells in the middle region of petioles where these cells could be easily observed in unstained petioles using bright-field microscopy. No significant difference in cell size was observed between the wild-type and sob3-6 petioles (Figures 1C and 1D), indicating that the long-petiole phenotype in sob3-6 is the result of increased cell division. SOB3-D, on the other hand, exhibits a 26%

decrease in average cell size compared with the wild-type. However, this change in cell size does not fully explain the 43% reduction in petiole length for SOB3-D compared with the wildtype (Figure 1B), suggesting that both cell expansion and cell number are altered in this mutant. Taken together, these results suggest that AHLs affect both cell elongation and cell division in petioles. However, as cortex cells near both the base of the petiole and the petiole-blade junction are difficult to observe using this approach, we only measured cell size in the middle region of the petiole. Therefore, this left open the possibility that differences in cell size at either end of the petiole cause the sob3-6 phenotype. To address this issue, we next measured cell size in calcoflour white-stained petioles observed with a confocal microscope. Despite measuring cells along the entire length of the petiole using this approach, we still observed no increase in cell size for sob3-6 (Figure S1B). However, a significant increase in cell numbers was observed for petioles of sob3-6 compared with the wild-type (Figure S1C). This finding further supports the hypothesis that the sob3-6 long-petiole phenotype is caused completely by increased cell division rather than enhanced cell growth. Also in agreement with the results obtained from the first experiment, cell size and number are both reduced in SOB3-D compared with the wild-type (Figures S1B and S1C). Therefore, we conclude that cell growth and division are both affected by AHLs in petioles.

AHLs Directly Repress Genes Associated with Growth and Development

Because AHLs are known to regulate gene transcription [9, 12, 13, 16, 25], we sought to identify genes downstream of these

transcription factors that could be responsible for the petiole phenotypes described above. Therefore, we examined gene expression in juvenile rosettes of SOB3-D and sob3-6 grown in long days (16 h light/8 h darkness) and harvested 4 h after lights on (ZT4), which is approximately the time when elongation growth in the leaf is maximal (Data S1) [32]. RNA sequencing (RNA-seq) analysis identified 3,851 AHL-regulated genes differentially expressed between SOB3-D and sob3-6 (Data S1A and S1B). Among these, we observed that the number of AHLrepressed genes (2,443) is nearly double that of AHL-induced genes (1,408). Gene ontology (GO) enrichment analysis indicated that among AHL-repressed genes, the terms "cellular process," "multicellular organismal process," "anatomical structure development," and "developmental process" are the most highly enriched (Data S1C). On the other hand, the most enriched GO terms among AHL-induced genes include "response to stimulus," "response to abiotic stimulus," "response to chemical stimulus," and "response to stress" (Data S1D). Taken together, these results suggest that AHLs activate stress responses while repressing growth.

Next, in order to identify direct downstream targets of AHLs, we analyzed genome-wide binding of SOB3 in planta (Data S2). Chromatin immunoprecipitation followed by sequencing (ChIP-seq) was performed using the previously published ProSOB3::SOB3-GFP sob3-4 line [16]. This ChIPseg analysis revealed binding of SOB3 to 9,980 loci (Data S2A). Consistent with the role of SOB3 as a transcription factor, the majority of binding events (52.4%) occur within -1 kb to +100 bp of a transcription start site (Promoter-TSS category in Figure 2A). Conversely, few binding events are observed in gene bodies, with only 5.1% of binding events occurring in introns and 1.4% in exons (Figure 2A). Annotation of ChIP-seq peaks identified a set of 7,427 SOB3-bound genes (Data S2A and 2B). Out of the AHL-repressed genes identified from RNA-seq, about 25% were also identified as SOB3-bound genes, suggesting that these 667 genes are directly repressed by SOB3 and possibly other AHLs (Figure 2B; Data S2D). When compared with AHL-repressed genes, a higher proportion (approximately 50%) of AHL-induced genes were identified as direct targets (Figure 2C; Data S2E). However, the total number of AHL-induced, SOB3-bound genes (719) does not differ drastically from the number of direct-target AHL-repressed genes, indicating that these transcription factors can act as both activators and repressors. Among genes directly repressed by AHLs, the GO terms "developmental process," "anatomical structure development," and "multicellular organismal process" are the most highly enriched (Figure 2D; Data S2F). Terms consistent with the petiole growth phenotypes observed for SOB3-D and sob3-6 (Figure 1) are also enriched, including "response to auxin stimulus," "regulation of cell size," and "response to brassinosteroid stimulus" (Figure 2D; Data S2F). "Response to stimulus," "response to chemical stimulus," and "response to abiotic stimulus" are the most highly enriched among AHL-induced direct targets (Figure 2E; Data S2G). Interestingly, the term "response to light stimulus" is enriched among both AHL-repressed and AHL-induced direct targets (Figures 2D and 2E; Data S2F and S2G). This finding is consistent with previous reports of light-dependent hypocotyl phenotypes in ahl mutants [17-19].

Next, in order to identify candidate cis elements bound by SOB3, we used DREME to conduct ab initio motif enrichment analysis [33] (Figure 2F; Data S2H). Interestingly, GGHCCA, which resembles motifs bound by TCP transcription factors [34-37], was identified as the most enriched motif (Figure 2F; Data S2H and S2I). Such a motif is likely bound by TCPs found in the same protein-DNA complex with SOB3, as it has been reported that AHLs and TCPs interact physically, and, further, that these interactions are biologically relevant in the context of hypocotyl growth [9, 38]. Therefore, the strong enrichment of this motif in regions bound by SOB3 strongly suggests that our ChIP-seq data are of good quality. On the other hand, the third-ranked motif, AWATAWTA, is a solid candidate for SOB3 binding, as it resembles sequences known to be bound by other members of the AHL family [34, 35] (Figure 2F; Data S2H and S2I). Further, the AT-hook, by which AHLs bind DNA [8, 9, 12, 25], is known to bind selectively to sequences containing A-T base pairs [39, 40]. Finally, AWATAWTA is highly centrally enriched within the 300 bp regions surrounding the summits of ChIP-seg peaks identified for SOB3-GFP (Figure S2) [41], further supporting the hypothesis that this motif is a binding site for SOB3. Three additional motifs identified via DREME, TAA-TAWTA, AWTAAATA, and ABAAAATA, also contain mainly A-T base pairs and exhibit strong central enrichment (Data S2H; Figure S2), indicating these motifs are also good candidates for cis-elements bound by SOB3.

AHLs and PIFs Have Opposite Effects on Petiole Growth

The second-ranked motif from enrichment analysis, CACRYG, resembles sequences bound by bHLH transcription factors, including MYCs and PIFs [34, 35, 42-47] (Data S2H and S2I). Given that PIFs are known to promote petiole elongation by activating auxin signaling [4, 48], we hypothesized that AHLs may influence petiole growth by antagonizing PIFs. Loss-of-function pif mutants, including pif4-101, are known to exhibit reduced petiole elongation [3, 4, 48, 49]. Strikingly, we found that in our growth conditions, pif4-101 has short petioles and reduced cell length, which both resemble SOB3-D phenotypes (Figures 1, S1A, and S1B). These data indicate that PIF4 promotes petiole growth at least in part by enhancing cell expansion. This result is unsurprising considering that PIFs have long been thought to promote hypocotyl elongation by enhancing cell growth [5, 45, 50]. More interestingly, we also observed that pif4-101 petioles exhibit a decrease in cell numbers, indicating that PIFs can also promote organ growth by increasing cell division (Figure S1C). Finally, our observations that SOB3-D and pif4-101 have comparable effects on petiole length, cell growth, and cell number (Figures 1 and S1) collectively suggest that AHLs may inhibit growth by repressing PIF activity.

AHLs Repress PIF-Activated Genes

We next investigated whether PIFs oppositely regulate any of the genes identified above as AHL-regulated genes. In order to generate a list of PIF-regulated genes in juvenile rosettes, RNA-seq was performed in the *pif4 pif5 pif7* triple mutant [48], which exhibits a similar short-petiole phenotype as *pif4-101* in our growth conditions (Figure S1A; Data S3). 336 and 79 genes were identified as induced and repressed by PIFs, respectively (Data S3A and S3B). Interestingly, among PIF-induced and

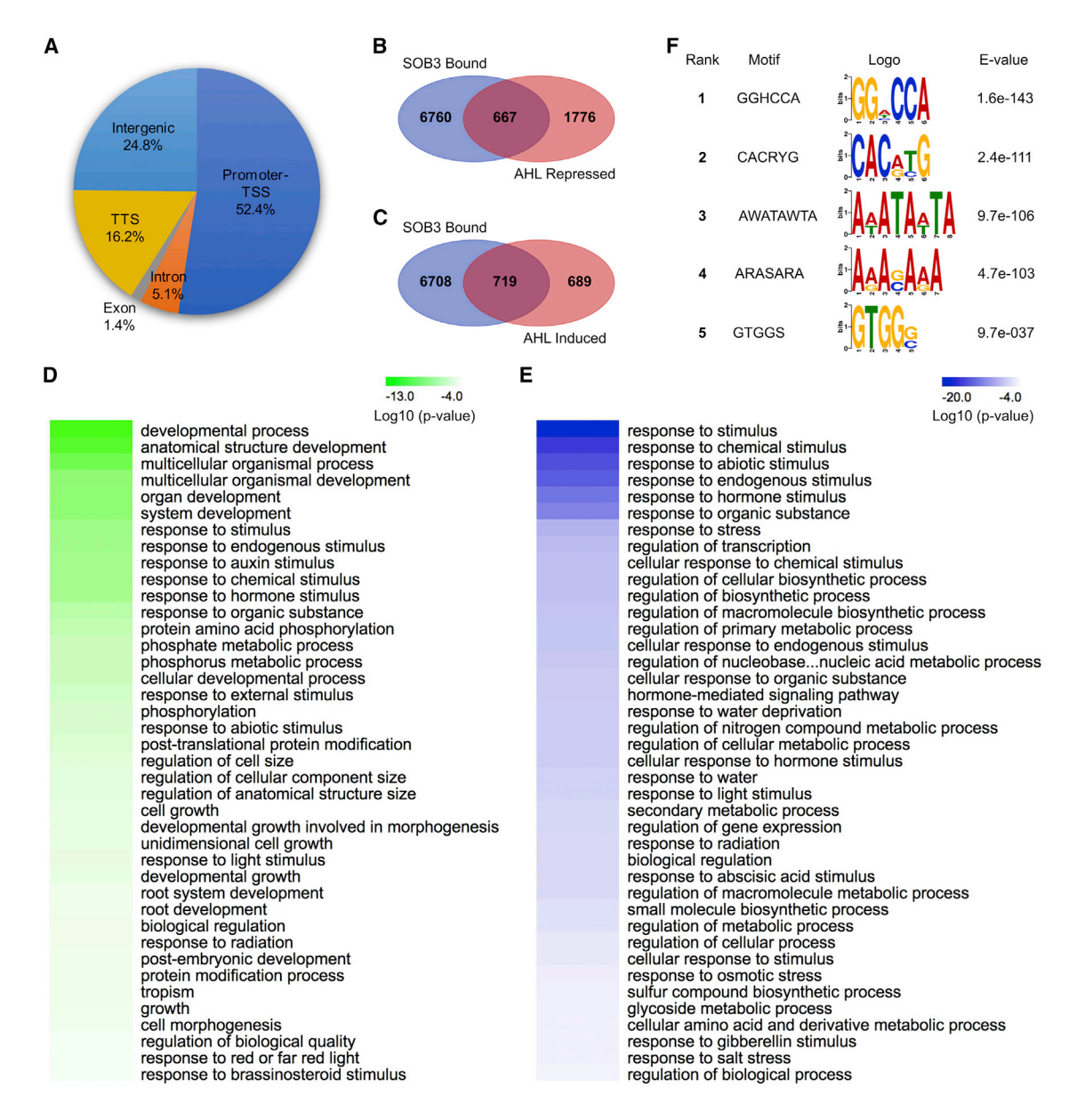


Figure 2. AHLs Directly Repress Genes Associated with Growth and Development

(A) Distribution of SOB3 binding sites determined from ChIP-seq data based on annotations obtained using HOMER software. "Promoter-TSS" is defined as -1,000 bp to +100 bp in relation to the transcription start site. "TTS" is defined as -100 bp to +1,000 bp in relation to the transcription termination site. (B and C) Overlap between genes bound by SOB3, based on ChIP-seq data, and those repressed (B) or induced (C) by AHLs, based on RNA-seq data. (D and E) Top 40 enriched GO terms for genes bound by SOB3 and also repressed (D) or induced (E) by AHLs. (F) Top 5 enriched motifs in the 100 bp regions surrounding SOB3 peaks, as determined using DREME [33]. See also Figure S2, Data S1, and S2.

PIF-repressed genes, we observed an enrichment of AHL-repressed and AHL-induced genes, respectively (Figures 3A and 3B). Among 336 PIF-induced genes, approximately 40% (134 genes) are also included in the list of AHL-repressed genes at the same time point (Figure 3A; Data S4A). A similar proportion of PIF-repressed genes are also induced by AHLs (43%, 34 of 79 genes) (Figure 3B; Data S4B). GO analysis revealed that among PIF-induced AHL-repressed genes, the GO terms "response to auxin stimulus," "response to stimulus," "response to organic

stimulus," and "response to hormone stimulus" are the most highly enriched (Figure 3C; Data S4C). Further, among the list of PIF-induced AHL-repressed genes, several have been previously identified as direct targets of PIFs, including 1-AMINO-CYCLOPROPANE-1-CARBOXYLATE SYNTHASE 8 (ACS8), ARABIDOPSIS THALIANA HOMEOBOX PROTEIN 2 (ATHB2), INDOLE-3-ACETIC ACID INDUCIBLE 19 (IAA19), IAA29, LONGIFOLIA 1 (LNG1), and YUCCA8 (YUC8) (Data S4A) [42, 45, 51–58]. Other enriched terms consistent with the petiole

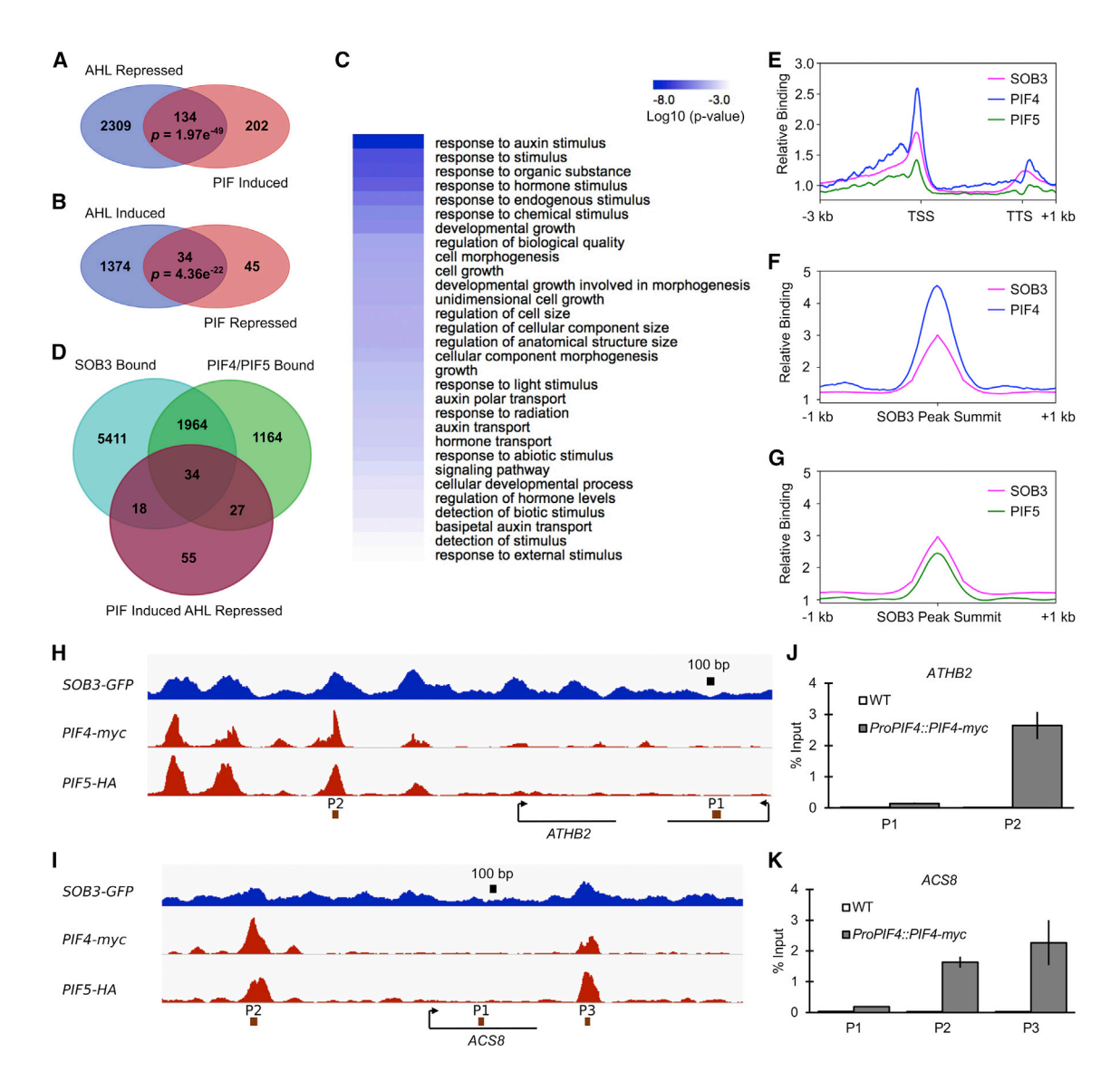


Figure 3. AHLs Repress PIF-Activated Genes

(A and B) Overlap between PIF-induced and AHL-repressed genes (A) or between PIF-repressed and AHL-induced genes (B), based on RNA-seq data. Significance of overlap between sets of differentially expressed genes was evaluated using the hypergeometric test.

(C) Top 30 enriched GO terms for PIF-induced AHL-repressed genes from (A).

(D) Overlap between genes bound by SOB3, genes bound by PIF4 and/or PIF5, and PIF-induced AHL-repressed genes from (A). SOB3-bound genes were identified based on our ChIP-seq data. PIF4- and PIF5-bound genes were identified based on our analysis of previously published ChIP-seq data [42, 45]. (E) Distribution of SOB3, PIF4, and PIF5 binding, based on the ChIP-seq data described above, for genes which are bound by SOB3 plus PIF4 and/or PIF5. (F and G) Distribution of SOB3 and PIF4 (F) or PIF5 (G) binding within the 2,000 bp regions surrounding summits of peaks identified from our SOB3 ChIP-seq data that are associated with genes also bound by the specified PIF.

(H and I) Binding of SOB3, PIF4, and PIF5 to loci associated with ATHB2 (H) or ACS8 (I), based on the ChIP-seq data described above. Black lines indicate positions of genes with attached arrows denoting transcription start sites.

(J and K) Binding of PIF4-myc to ATHB2-associated (J) or ACS8-associated (K) loci, based on ChIP-qPCR data. Positions of primers relative to the ATHB2 and ACS8 genes are depicted by brown bars in (H) and (I), respectively. Bar graph values represent means of two biological replicates for each genotype and error bars represent SEM.

See also Figure S3, Data S3, and S4.

phenotypes observed in *ahl* and *pif* mutants include "cell growth," "response to light stimulus," and "auxin polar transport" (Figure 3C; Data S4C). On the other hand, *HY5-HOMOLOG* (*HYH*), which is known to repress growth in hypocotyls grown under blue light [59], is among the PIF-repressed AHL-induced

genes (Data S4B). These results indicate that AHLs oppositely affect the transcription of many PIF-regulated genes.

We also investigated whether SOB3 and PIFs bind to similar sets of genes. To this end, we re-analyzed previously published ChIP-seq data for PIF4 [45] and PIF5 [42], using the

same analysis pipeline as we did for our SOB3 ChIP-seq data. Based on these data, we identified 3,189 genes bound by PIF4 and/or PIF5 (Data S4D and S4E), a substantial proportion (1,998 genes = 63%) of which are also bound by SOB3 based on our ChIP-seq data (Figures 3D and S3A; Data S4F). We next investigated whether SOB3 and PIFs bind to similar loci associated with genes which are bound by both transcription factors. All three transcription factors exhibit similar distributions of binding to genes that are bound by both SOB3 and PIFs, with binding frequently observed in the promoter region, particularly just upstream of the transcription start site (TSS) (Figure 3E). In order to further investigate the overlap between SOB3 and PIF binding sites, we investigated whether PIF binding is enriched in the 2,000 bp regions surrounding the summits of SOB3 ChIP-seq peaks associated with genes that are bound by both transcription factors. Based on these analyses, we found that binding of both PIF4 (Figure 3F) and PIF5 (Figure 3G) is substantially enriched in the vicinity of SOB3 peak summits. These results indicate that SOB3 and PIFs bind preferentially to similar regions in genes that are bound by both transcription factors. Therefore, AHLs may affect petiole growth by directly binding to PIF-regulated genes and antagonizing the ability of PIFs to exert their effect on gene transcription. To test this hypothesis, we compared the RNA-seg and ChIP-seg data. Among genes bound by SOB3 plus PIF4 and/or PIF5, we found that 34 are also PIFinduced and AHL-repressed based on the RNA-seq data (Figure 3D; Data S4G). This is substantially more than the number of transcribed SOB3- and PIF-bound genes expected by chance to be both induced by PIFs and repressed by AHLs (Figure S3B). Several of these 34 genes are associated with growth and auxin transport, homeostasis, or response, including ATHB2, GRETHCEN HAGEN 3.6 (GH3.6), IAA19, NAKED PINS IN YUC MUTANTS 1 (NPY1), PIN-FORMED 3 (PIN3), SMALL AUXIN UP RNA 24 (SAUR24), YUC8, and WALLS ARE THIN 1 (WAT1) (Data S4G; Figures 3H, S3C, and S3D) [51, 52, 60-70]. Notably, another gene included in this list encodes PLASMA MEMBRANE PROTON ATPASE 2 (AHA2), which is activated at the protein level by SAURs and enhances cell growth by directly promoting acidification of the apoplast [61]. Brassinosteroids and ethylene are known to promote petiole growth [71, 72], and we also found genes associated with brassinosteroid perception (BRI1) [73] and ethylene biosynthesis (ACS8) [74] in the list of PIF-induced AHL-repressed genes bound by both transcription factors (Data S4G; Figure 3I). In order to confirm that PIF4 is able to bind to some of these targets in our experimental conditions and at the time point used for our RNA-seq experiment, we next performed ChIP-qPCR using a ProPIF4::PIF4-myc line. Our ChIP-qPCR results indicate that PIF4 binds to loci associated with ACS8, ATHB2, SAUR24, and YUC8 in long daygrown juvenile rosettes at ZT4 (Figures 3H-3K and S3C-S3F). Collectively, these data suggest that SOB3 modulates petiole growth by directly repressing the transcription of genes activated by PIFs, particularly those associated with hormone signaling pathways. Further, our results suggest that SOB3 exerts its effect on growth mainly by acting on hormone signaling pathways, rather than by directly affecting genes involved in regulation of cell growth and proliferation.

The Effect of SOB3 on Petiole Growth Is Dependent on PIF4

In order to further test the hypothesis that AHLs influence growth by antagonizing PIF activity, we crossed sob3-6 into two loss-offunction mutants for PIF4, pif4-101 [49], and pif4-2 [75]. We observed no significant increase in petiole growth for the pif4-101 sob3-6 and pif4-2 sob3-6 double mutants compared with their respective pif4 single mutants (Figures 4A and 4B). This indicates that a reduction in PIF activity abolishes the ability of sob3-6 to confer enhanced growth, consistent with the idea that SOB3 modulates petiole elongation by antagonizing PIFmediated transcriptional activation. Similarly, we observed that the removal of PIF4 is epistatic to sob3-6 regarding the expression of four genes directly regulated by SOB3 and PIFs, ACS8, ATHB2, CAD7, and NPY1 (Data S4G; Figures 3H-3K and 4C). Although the expression of these genes is elevated in sob3-6, transcript levels are similarly depleted compared with the wildtype in both pif4-101 and pif4-101 sob3-6. One potential explanation for the epistatic nature of pif4 mutants over sob3-6 is that AHLs repress PIF transcription. However, according to our RNAseg data, out of the six PIFs known to promote elongation growth [6, 55, 76, 77], PIF3, PIF4, PIF5, PIF7, and PIF8 transcript levels are not significantly altered in SOB3-D or sob3-6, while PIF1 expression is altered in a manner consistent with transcriptional activation by AHLs (Data S1E-S1G). Therefore, these results indicate that, at least under the growth conditions used for our phenotypic analyses, AHLs do not repress petiole growth by inhibiting PIF transcription. Another possibility is that AHLs affect PIF4 accumulation at the protein level. In order to test this possibility, we generated a ProPIF4::PIF4-myc XVE::SOB3 line, in which SOB3 expression can be induced by addition of 17β-estradiol (Figure S4A). PIF4-myc protein levels were then examined, using an anti-myc tag antibody, following SOB3 induction (Figure 4D). We observed that nearly 70% less of the PIF4-myc protein is detected in ProPIF4::PIF4-myc XVE::SOB3 compared with ProPIF4::PIF4-mvc following approximately two days of growth on estradiol-containing medium, indicating that SOB3 induction drastically inhibits PIF4 protein accumulation (Figures 4D and 4E). This finding is further supported by the observation that such a decrease in PIF4-myc protein is not observed in mock-treated ProPIF4::PIF4-myc XVE::SOB3 plants (Figures 4D and 4E). We further investigated whether this decrease in PIF4 protein could be due to an effect of SOB3 induction on PIF4 transcription. In plants grown on estradiol, we observed a 33% decrease in the PIF4 transcription in ProPIF4::PIF4-myc XVE::SOB3 versus ProPIF4::PIF4-myc, although this change is not quite significant (p = 0.0754; Figure S4B). Our ChIP-seq data additionally indicate that SOB3 can bind both upstream and downstream of PIF4 (Figure S4C; Data S2A and S2B). These data suggest that SOB3 may directly repress PIF4 transcription under certain conditions, which may partially explain the decrease in PIF4-myc observed in ProPIF4::PIF4-myc XVE::SOB3 grown on inducible medium (Figures 4D and 4E).

SOB3 Reduces Binding of PIF4 to Target Loci

The observed binding of SOB3 and PIF4 to similar loci (Figures 3E–3K and S3C–S3F) suggests that potentially the two transcription factors bind to DNA as a complex and engage in protein-protein

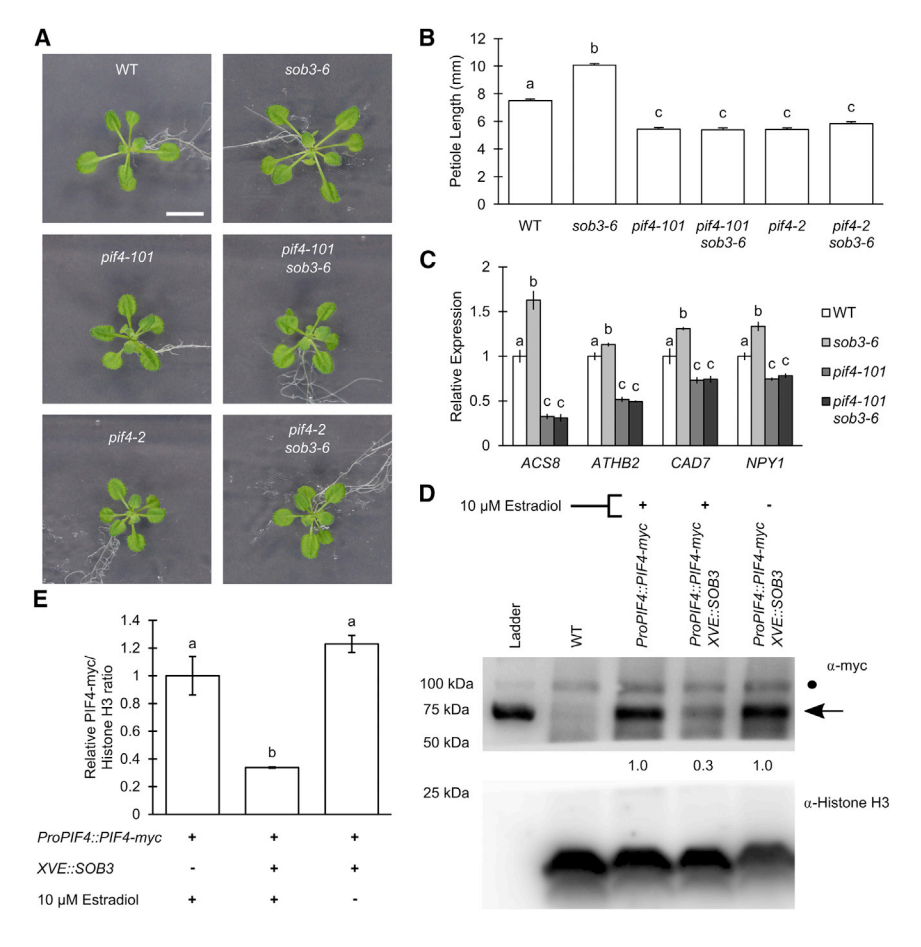


Figure 4. The Effect of SOB3 on Petiole Growth Is Dependent on PIF4

(A and B) Petiole phenotypes indicate that *pif4* is epistatic over *sob3-6*. (A) Representative juvenile rosettes for *sob3-6*, *pif4*, and *pif4 sob3-6* mutants as well as the WT, Col-0. Scale bar, 10 mm. (B) Quantification of leaf 4 petiole lengths for 21-day-old plants of the genotypes pictured in (A). Bar graph values represent means of measured petiole lengths for each genotype and error bars represent SEM. Different letters indicate significant differences based on one-way ANOVA with Tukey's HSD test (p < 0.001).

(C) Gene expression data indicate that *pif4* is epistatic over *sob3-6*. Relative transcript levels of *ACS8*, *ATHB2*, *CAD7*, and *NPY1* in 14-day-old juvenile rosettes measured by qRT-PCR. Bar graph values represent means expressed as relative change compared with the WT and error bars represent SEM. Different letters indicate significant differences between genotypes based on one-way ANOVA with Tukey's HSD test (p < 0.05).

(D and E) SOB3 induction reduces PIF4-myc protein accumulation. (D) Representative western blot images showing a decrease in PIF4-myc protein following approximately two days of SOB3 induction. PIF4-myc was detected using an α -myc antibody. The arrow denotes PIF4-myc protein, while the dot indicates non-specific binding by the α -myc antibody. α -Histone H3 was used as a loading control for nuclear proteins. Numbers indicate ratio of PIF4-myc/Histone H3 detected relative to the ProPIF4::PIF4-myc sample. (E) Quantitative data from three biological replicates, where PIF4-myc levels were estimated using the approach described in (D). Bar graph values represent relative change in PIF4-myc/Histone H3

ratio compared with the *ProPIF4::PIF4-myc* samples and error bars represent SEM. Different letters indicate significant differences between genotypes based on one-way ANOVA with Tukey's HSD test (p < 0.01).

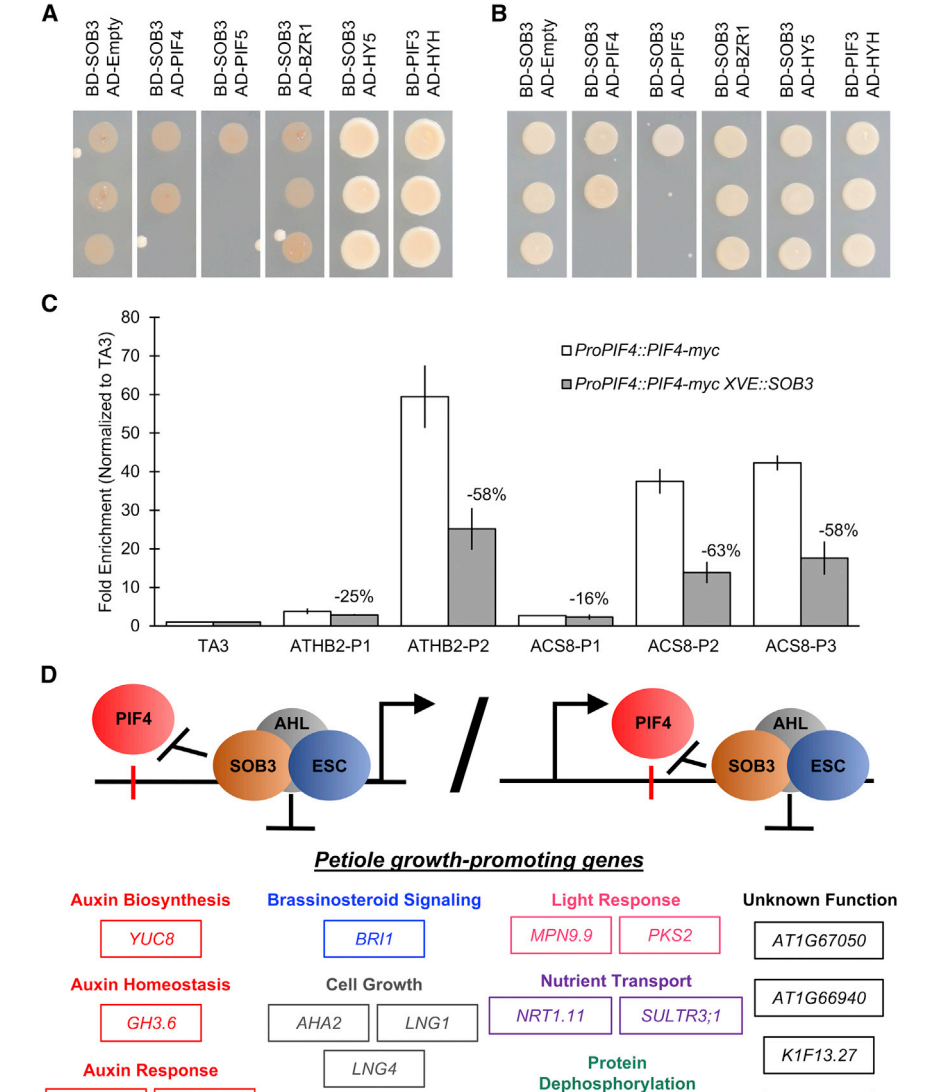
See also Figure S4.

interactions with each other. Therefore, we next examined the potential interaction between SOB3 and PIFs using yeast two-hybrid (Y2H). However, no interaction was observed between SOB3 and PIF4 in two different Y2H systems (Figures 5A and 5B, S5A, and S5B). We also failed to observe an interaction between SOB3 and PIF5 (Figures 5A and 5B). Another possibility is that rather than binding in a complex together with PIF4, SOB3 reduces PIF4 binding to DNA, which would be consistent with the observed decrease in PIF4-myc protein following SOB3 induction (Figures 4D and 4E). Therefore, we examined the effect of SOB3 induction on PIF4-myc binding to direct target genes via ChIP-qPCR. Following approximately two days of growth on inducible medium, we observed less binding of PIF4-myc to target genes in ProPIF4:: PIF4-myc XVE::SOB3 plants as compared with the ProPIF4::PIF4myc control (Figures 5C and S5C). Consistent with the finding that SOB3 reduces PIF4 protein accumulation (Figures 4D and 4E), we observed decreased PIF4-myc binding both at loci bound by SOB3, such those associated with ACS8 and ATHB2, and at regions only bound by PIF4, as in the promoters of HIPP27 and BZIP75 (Figures 3H-3K, 5C, S3C-S3F, and S5C-S5E). However, a more substantial reduction in PIF4-myc binding was observed at the loci bound by both types of transcription factors as compared with those only bound by PIF4. This suggests

that SOB3 may further reduce PIF4 occupancy at these loci by competing with PIFs for binding to similar DNA regions. Collectively, our data point to a model whereby AHLs reduce PIF occupancy of DNA, particularly at loci bound by both types of transcription factors, thus repressing the transcription of growth-promoting genes, and, consequently, petiole elongation (Figure 5D).

DISCUSSION

In this study, we demonstrated that SOB3 and other AHLs influence petiole growth by reducing PIF binding to and transcriptional activation of genes associated with hormone signaling pathways (Figure 5D). Previous work has indicated that SOB3 represses auxin signaling by affecting transcription of *YUC8*, involved in auxin biosynthesis, and members of the *SAUR19* subfamily, which act downstream of the auxin signaling pathway [16]. Our findings herein indicate that AHLs exert an additional repressive effect on auxin signaling by inhibiting the transcription of genes that affect auxin transport, including *NPY1* [64–67] (Data S4G; Figure 4C). We also obtained evidence suggesting that AHLs can repress growth by suppressing ethylene production via repression of *ACS8* [74] (Data S4G; Figures 3I and 4C).



Additionally, our finding that AHLs repress expression of the brassinosteroid receptor-encoding BRI1 gene [73] (Data S4G) provides further insight into a previously reported interaction between this hormone signaling pathway and the AHLs [17]. In addition to their effect on PIF-mediated hormone signaling, we also found that AHLs influence the expression of a large number of genes not regulated by PIFs (Figures 3A and 3B). Therefore, an important topic for future studies is investigating the biological consequences resulting from the AHL regulation of PIF-independent targets. It will be interesting to investigate, for example, whether SOB3 can also repress growth by acting on PIF-independent pathways.

Cell Wall Metabolism

Ethylene Biosynthesis

ACS8

CAD7

FAR1

T32A16.3

UGT72E1

ATHB2

IAA19

NPY1

PIN7

1442

SAUR24

PIN3

WAT1

Auxin Transport

Figure 5. SOB3 Interferes with Binding of PIF4 to Target Loci

(A and B) SOB3 does not interact with PIF4 or PIF5 in the Matchmaker Gold Yeast Two-Hybrid system, while a positive interaction is detected with HY5. Images depict the binding assay performed on SD medium lacking tryptophan, leucine, histidine, and adenine (A) or prior growth of the same yeast on a control plate containing SD medium without tryptophan and leucine (B). Only two or one biological replicate(s) are shown for PIF4 or PIF5, respectively, because of extremely low transformation efficiencies in this system. PIF3-HYH binding was used as a positive control.

(C) PIF4-myc binding to loci associated with ATHB2 or ACS8 is reduced following approximately 2 days of SOB3 induction, based on ChIPqPCR data. Positions of primers relative to the ATHB2 and ACS8 genes are depicted by brown bars in Figures 3H and 3I, respectively. Bar graph values represent means of two biological replicates for each genotype and error bars represent SEM. Percentages depict percent differences in enrichment for ProPIF4::PIF4-myc XVE::SOB3 relative to ProPIF4::PIF4-myc.

(D) A model depicting how AHLs repress petiole growth by reducing PIF occupancy at growthpromoting genes, thus inhibiting their transcriptional activation. Red vertical bars depict PIF binding sites.

See also Figure S5.

F10B6.30

MMI9.11

MYOB2

IQD28

APD7

Receptor Kinase

Shoot Development

RTFL16

CEPR2

Another important theme for future studies is elucidating the precise molecular mechanism by which AHLs inhibit PIFmediated activation of gene transcription. Our data suggest that AHLs may inhibit PIFs via multiple mechanisms. First, in AHLs cases, may directly inhibit the transcription of PIFs. SOB3 binds to the promoter of PIF4 as well as immediately downstream of this gene, and we observed a 33% decrease in the expression of PIF4 in ProPIF4::PIF4myc XVE::SOB3 compared with Pro-PIF4::PIF4-myc grown on estradiol-containing medium (Figures S4B and S4C; Data S2A and S2B). Additionally, SOB3 binds to PIF1, PIF3, PIF5, PIF7, and

PIF8, suggesting that in some cases, AHLs may also directly regulate the transcription of these PIFs (Figure S4D; Data S2A and S2B). However, it is important to note that an effect of AHLs on PIF transcription does not account for the petiole phenotypes observed in sob3-6 and SOB3-D (Figures 1 and S1; Data S1E-S1G). Data from our RNA-seq experiment, which was performed under the same growth conditions as the phenotypic studies, indicate that none of the PIFs exhibit a substantial decrease or increase in expression in SOB3-D or sob3-6, respectively (Data S1E-S1G). The experiment investigating PIF4 expression following induction of SOB3 (Figures S4A and S4B), on the other hand, was performed using light with a higher

fluence rate, in order to compensate for the fact that the Pro-PIF4::PIF4-myc and ProPIF4::PIF4-myc XVE::SOB3 lines contain extra copies of the PIF4 gene (See STAR Methods). Therefore, one possibility is that SOB3, and potentially other AHLs, specifically inhibit PIF transcription in plants growing in light of higher fluence rates. However, our data also indicate that AHLs likely inhibit PIF protein activity independently of their effect on PIF transcription. In ProPIF4::PIF4-myc XVE::SOB3 compared with ProPIF4::PIF4-myc grown on inducible medium, we observed a more dramatic reduction in the PIF4-myc protein level and binding of this transcription factor to genes like ATHB2 and ACS8 than the change in PIF4 expression between these two lines (Figures 4D and 4E, 5C, S4B, and S5C). Further, PIF4-myc binding to target loci in ProPIF4::PIF4-myc XVE::SOB3 is reduced more substantially at loci which are also bound by SOB3 (Figures 3H, 3I, 5C, S3C, S3D, and S5C-S5E). This last observation suggests that SOB3 binding at loci targeted by both types of transcription factors can physically block PIF binding to DNA. Based on these observations, we propose that the petiole phenotypes observed in SOB3-D and sob3-6 grown under relatively dim light are because of a repressive effect of AHLs on PIFs at the protein level (Figure 5D).

There are a few potential ways in which AHLs could affect PIF activity. PIF protein stability is regulated by several different mechanisms and factors [78]. Therefore, AHLs may indirectly promote PIF degradation by affecting the transcription of one or more factors that affect its stability. One possibility is that AHLs promote PIF degradation by promoting BRASSINOSTEROID-INSENSITIVE 2 (BIN2)-mediated phosphorylation, which is known to promote degradation of PIF3 and PIF4 [79, 80]. Our RNA-seq data indicate that BIN2 is upregulated in SOB3-D compared with sob3-6 (Data S1E), and binding of SOB3 to the BIN2 promoter was detected in our ChIP-seq data (Figure S4E; Data S2A and S2B), indicating that AHLs promote transcription of this kinase. Additionally, as mentioned previously, we found that AHLs directly repress the expression of BRI1 (Data S4G). Therefore, AHLs could also promote PIF phosphorylation and degradation by attenuating BRI1-dependent degradation of the BIN2 kinase in response to brassinosteroids [81]. Another possibility is that AHLs destabilize PIFs by promoting the expression of REPRESSOR OF GA (RGA), a DELLA protein which serves as a repressor of the gibberellic acid (GA) signaling pathway [82-84]. DELLAs interact with PIFs, including PIF4, and promote their degradation, while also inhibiting their ability to bind DNA [50, 85, 86]. We observed enhanced expression of RGA in SOB3-D compared with sob3-6, as well as binding of SOB3 both upstream and downstream of this gene (Figure S4F; Data S1E, S2A, and S2B). Collectively, these data indicate that AHLs may promote DELLA-mediated degradation and/or sequestration of PIFs by increasing RGA transcription. It is further possible that AHLs reduce PIF4 stability by interfering with its ability to activate target gene expression, as there is evidence that this PIF is specifically stabilized by functioning as a transcriptional activator [87]. There are a few potential ways in which AHLs could directly interfere with PIF binding to target loci, although the two types of transcription factors bind different types of DNA sequences [8, 9, 12, 25, 39, 40, 42, 44-47]. Binding of an AT-hook is known to induce bending in DNA [88]. Therefore, one possibility is that AHL-DNA interactions simply contort loci bound by PIFs, destabilizing the binding of these transcription

factors. Another mutually non-exclusive possibility is that AHLs function as part of a transcriptional repressor complex together with other transcription factors, which themselves also directly regulate PIF direct targets, such as TCPs, BZR1, or HY5 [45, 89–93]. This seems like an especially good possibility, considering that AT-hook motifs are known to bind promiscuously to short stretches of AT base pairs [40], and, therefore, it is likely that another factor is needed to target AHLs to specific loci. We observed that motifs associated with TCP binding are enriched in SOB3-bound regions (Figure 2F). Further, it has been previously shown that the sob3-6 long hypocotyl phenotype is completely abolished in the TCP-deficient jaw-D background [9, 94], suggesting that TCPs could play a role in AHL-mediated repression of PIF targets, possibly by targeting them to PIF-bound loci. Similar to a previous report that AHLs and TCPs interact in Y2H [9], we found that SOB3 can interact with HY5; however, we failed to detect an interaction with BZR1 (Figures 5A, 5B, S5A, and S5B). Notably, it has been shown than HY5 and PIF1 antagonistically regulate PSY expression by competitively binding to a G-box motif located in its promoter [89]. Further, there is evidence that YUC8 is regulated in a similar antagonistic fashion by competitive binding of HY5 and PIF4 to a region within the promoter where we also observed the binding of both SOB3 and PIF4 in this study [90] (Figures S3D and S3F). Therefore, it is possible that SOB3 forms a protein-DNA complex together with HY5, which competitively inhibits binding of PIF4 to its target genes.

Finally, the AHL-focused work in this study together with several previous findings [50, 79, 85, 95-105] have collectively demonstrated that PIF activity is attenuated via multiple pathways, highlighting the remarkable complexity by which these central regulators of growth are controlled. It is interesting to note in this context that AHLs are activated in response to a variety of different types of abiotic stress, including drought, salt, and cold stress [29-31]. A suite of regulatory mechanisms for PIFs likely enables stress-responsive factors, such as the AHLs, to restrict plant growth when resources need to be diverted to any of a number of different types of stress responses. This is analogous to DELLA-mediated inhibition of PIF activity, which is promoted by the stress-responsive jasmonate signaling pathway [106]. By affecting PIF activity, AHLs are ideally placed to function as key components of gene regulatory networks, controlling plant growth in response to a variety of external stimuli.

STAR*METHODS

Detailed methods are provided in the online version of this paper and include the following:

- KEY RESOURCES TABLE
- LEAD CONTACT AND MATERIALS AVAILABILITY
- EXPERIMENTAL MODEL AND SUBJECT DETAILS
 - Plant materials and growth conditions
- METHOD DETAILS
 - O Petiole and cell measurements
 - mRNA extraction
 - RNA sequencing and data analysis
 - $\, \bigcirc \,$ Real-time quantitative reverse transcription PCR
 - Chromatin immunoprecipitation sequencing

- ChIP-seq data analysis
- O ChIP-qPCR
- O Preparation of transgenic lines and mutants
- O Protein extraction and western blot
- Yeast two-hybrid
- QUANTIFICATION AND STATISTICAL ANALYSIS
- DATA AND CODE AVAILABILITY

SUPPLEMENTAL INFORMATION

Supplemental Information can be found online at https://doi.org/10.1016/j. cub 2020 02 017.

ACKNOWLEDGMENTS

We thank Christian Fankhauser (UNIL, Switzerland) for providing the pif4-101 and pif4 pif5 pif7 mutants, Peter Quail (UC Berkeley, USA) for the pif4-2 mutant, and Dr. Nobutaka Mitsuda (AIST, Japan) for the Y2H vectors harboring PIF3 or HYH. We thank the RIKEN CSRS Mass Spectrometry and Microscopy Unit for support with the imaging techniques and Dr. Yasuhiro Kadota (RIKEN Yokohama, Japan) for advice regarding the protein isolation and western blot procedures. We thank Noriko Doi and Chika Ikeda for technical assistance and current and former members of the Sugimoto and Wigge labs for useful technical advice, comments, and discussion. This work was supported in Japan by the Ministry of Education, Culture, Sports, Science and Technology (MEXT) (grant no. 15H05961 to K.S.) and the Japan Society for the Promotion of Science (JSPS) (grant no. 17H03704 to K.S. and fellowships to D.S.F.). This research was also supported by the United States Department of Agriculture (USDA) National Institute of Food and Agriculture (Hatch Umbrella Project #1015621 to M.M.N.).

AUTHOR CONTRIBUTIONS

 $Conceptualization\ and\ Methodology,\ D.S.F.,\ M.S.,\ P.A.W.,\ M.M.N.,\ and\ K.S.;$ Resources, D.S.F., J.-H.J., and T.I.; Investigation, D.S.F., A.K., M.S., A.T., T.S., and K.E.J.; Writing - Original Draft, D.S.F. and K.S.; Writing - Review & Editing: D.S.F., P.A.W., and K.S.; Funding Acquisition: D.S.F., M.M.N., and K.S.; Supervision: A.I., P.A.W., M.M.N., and K.S.

DECLARATION OF INTERESTS

The authors declare no competing interests.

Received: January 19, 2019 Revised: October 26, 2019 Accepted: February 6, 2020 Published: March 19, 2020

REFERENCES

- 1. Bechtold, U., and Field, B. (2018). Molecular mechanisms controlling plant growth during abiotic stress. J. Exp. Bot. 69, 2753-2758.
- 2. Huot, B., Yao, J., Montgomery, B.L., and He, S.Y. (2014). Growth-defense tradeoffs in plants: a balancing act to optimize fitness. Mol. Plant 7. 1267-1287.
- 3. Koini, M.A., Alvey, L., Allen, T., Tilley, C.A., Harberd, N.P., Whitelam, G.C., and Franklin, K.A. (2009). High temperature-mediated adaptations in plant architecture require the bHLH transcription factor PIF4. Curr. Biol. 19, 408-413.
- 4. de Wit, M., Keuskamp, D.H., Bongers, F.J., Hornitschek, P., Gommers, C.M.M., Reinen, E., Martínez-Cerón, C., Fankhauser, C., and Pierik, R. (2016). Integration of phytochrome and cryptochrome signals determines plant growth during competition for light. Curr. Biol. 26, 3320-3326.
- 5. Huq, E., and Quail, P.H. (2002). PIF4, a phytochrome-interacting bHLH factor, functions as a negative regulator of phytochrome B signaling in Arabidopsis. EMBO J. 21, 2441-2450.

- 6. Shin, J., Kim, K., Kang, H., Zulfugarov, I.S., Bae, G., Lee, C.H., Lee, D., and Choi, G. (2009). Phytochromes promote seedling light responses by inhibiting four negatively-acting phytochrome-interacting factors. Proc. Natl. Acad. Sci. USA 106, 7660-7665.
- 7. Paik, I., Kathare, P.K., Kim, J.I., and Huq, E. (2017). Expanding roles of PIFs in signal integration from multiple processes. Mol. Plant 10, 1035-
- 8. Fujimoto, S., Matsunaga, S., Yonemura, M., Uchiyama, S., Azuma, T., and Fukui, K. (2004). Identification of a novel plant MAR DNA binding protein localized on chromosomal surfaces. Plant Mol. Biol. 56, 225-239.
- 9. Zhao, J., Favero, D.S., Peng, H., and Neff, M.M. (2013). Arabidopsis thaliana AHL family modulates hypocotyl growth redundantly by interacting with each other via the PPC/DUF296 domain. Proc. Natl. Acad. Sci. USA 110. E4688-E4697.
- 10. Zhao, J., Favero, D.S., Qiu, J., Roalson, E.H., and Neff, M.M. (2014). Insights into the evolution and diversification of the AT-hook Motif Nuclear Localized gene family in land plants. BMC Plant Biol. 14, 266.
- 11. Lim, P.O., Kim, Y., Breeze, E., Koo, J.C., Woo, H.R., Ryu, J.S., Park, D.H., Beynon, J., Tabrett, A., Buchanan-Wollaston, V., and Nam, H.G. (2007). Overexpression of a chromatin architecture-controlling AT-hook protein extends leaf longevity and increases the post-harvest storage life of plants. Plant J. 52, 1140-1153.
- 12. Yun, J., Kim, Y.S., Jung, J.H., Seo, P.J., and Park, C.M. (2012). The AThook motif-containing protein AHL22 regulates flowering initiation by modifying FLOWERING LOCUS T chromatin in Arabidopsis. J. Biol. Chem. 287, 15307-15316.
- 13. Xu, Y., Wang, Y., Stroud, H., Gu, X., Sun, B., Gan, E.S., Ng, K.H., Jacobsen, S.E., He, Y., and Ito, T. (2013). A matrix protein silences transposons and repeats through interaction with retinoblastoma-associated proteins. Curr. Biol. 23, 345-350.
- 14. Jiang, H., Moreno-Romero, J., Santos-González, J., De Jaeger, G., Gevaert, K., Van De Slijke, E., and Köhler, C. (2017). Ectopic application of the repressive histone modification H3K9me2 establishes post-zygotic reproductive isolation in Arabidopsis thaliana. Genes Dev. 31, 1272-1287.
- 15. Lee, K., and Seo, P.J. (2017). Coordination of matrix attachment and ATP-dependent chromatin remodeling regulate auxin biosynthesis and Arabidopsis hypocotyl elongation. PLoS ONE 12, e0181804.
- 16. Favero, D.S., Jacques, C.N., Iwase, A., Le, K.N., Zhao, J., Sugimoto, K., and Neff, M.M. (2016). SUPPRESSOR OF PHYTOCHROME B4-#3 represses genes associated with auxin signaling to modulate hypocotyl growth. Plant Physiol. 171, 2701-2716.
- 17. Favero, D.S., Le, K.N., and Neff, M.M. (2017). Brassinosteroid signaling converges with SUPPRESSOR OF PHYTOCHROME B4-#3 to influence the expression of SMALL AUXIN UP RNA genes and hypocotyl growth. Plant J. 89, 1133-1145.
- 18. Street, I.H., Shah, P.K., Smith, A.M., Avery, N., and Neff, M.M. (2008). The AT-hook-containing proteins SOB3/AHL29 and ESC/AHL27 are negative modulators of hypocotyl growth in Arabidopsis. Plant J. 54, 1-14.
- 19. Xiao, C., Chen, F., Yu, X., Lin, C., and Fu, Y.F. (2009). Over-expression of an AT-hook gene, AHL22, delays flowering and inhibits the elongation of the hypocotyl in Arabidopsis thaliana. Plant Mol. Biol. 71, 39-50.
- 20. Xu, Y., Gan, E.S., and Ito, T. (2013). The AT-hook/PPC domain protein TEK negatively regulates floral repressors including MAF4 and MAF5. Plant Signal. Behav. 8, e25006.
- 21. Ng, K.H., Yu, H., and Ito, T. (2009). AGAMOUS controls GIANT KILLER, a multifunctional chromatin modifier in reproductive organ patterning and differentiation. PLoS Biol. 7, e1000251.
- 22. Gallavotti, A., Malcomber, S., Gaines, C., Stanfield, S., Whipple, C., Kellogg, E., and Schmidt, R.J. (2011). BARREN STALK FASTIGIATE1 is an AT-hook protein required for the formation of maize ears. Plant Cell 23, 1756-1771.

- Jin, Y., Luo, Q., Tong, H., Wang, A., Cheng, Z., Tang, J., Li, D., Zhao, X., Li, X., Wan, J., et al. (2011). An AT-hook gene is required for palea formation and floral organ number control in rice. Dev. Biol. 359, 277–288.
- Lou, Y., Xu, X.F., Zhu, J., Gu, J.N., Blackmore, S., and Yang, Z.N. (2014).
 The tapetal AHL family protein TEK determines nexine formation in the pollen wall. Nat. Commun. 5, 3855.
- Jia, Q.S., Zhu, J., Xu, X.F., Lou, Y., Zhang, Z.L., Zhang, Z.P., and Yang, Z.N. (2015). Arabidopsis AT-hook protein TEK positively regulates the expression of arabinogalactan proteins for Nexine formation. Mol. Plant 8, 251–260.
- Zhou, J., Wang, X., Lee, J.Y., and Lee, J.Y. (2013). Cell-to-cell movement of two interacting AT-hook factors in Arabidopsis root vascular tissue patterning. Plant Cell 25, 187–201.
- Lu, H., Zou, Y., and Feng, N. (2010). Overexpression of AHL20 negatively regulates defenses in Arabidopsis. J. Integr. Plant Biol. 52, 801–808.
- Yadeta, K.A., Hanemian, M., Smit, P., Hiemstra, J.A., Pereira, A., Marco, Y., and Thomma, B.P. (2011). The Arabidopsis thaliana DNA-binding protein AHL19 mediates verticillium wilt resistance. Mol. Plant Microbe Interact. 24, 1582–1591.
- Wong, M.M., Bhaskara, G.B., Wen, T.N., Lin, W.D., Nguyen, T.T., Chong, G.L., and Verslues, P.E. (2019). Phosphoproteomics of *Arabidopsis* Highly ABA-Induced1 identifies AT-Hook-Like10 phosphorylation required for stress growth regulation. Proc. Natl. Acad. Sci. USA *116*, 2354–2363.
- Zhou, L., Liu, Z., Liu, Y., Kong, D., Li, T., Yu, S., Mei, H., Xu, X., Liu, H., Chen, L., and Luo, L. (2016). A novel gene OsAHL1 improves both drought avoidance and drought tolerance in rice. Sci. Rep. 6, 30264.
- Shao, F., Zhang, L., Wilson, I.W., and Qiu, D. (2018). Transcriptomic analysis of *Betula halophila* in response to salt stress. Int. J. Mol. Sci. 19, 3412
- Dornbusch, T., Michaud, O., Xenarios, I., and Fankhauser, C. (2014).
 Differentially phased leaf growth and movements in Arabidopsis depend on coordinated circadian and light regulation. Plant Cell 26, 3911–3921.
- Bailey, T.L. (2011). DREME: motif discovery in transcription factor ChIPseq data. Bioinformatics 27, 1653–1659.
- Franco-Zorrilla, J.M., López-Vidriero, I., Carrasco, J.L., Godoy, M., Vera, P., and Solano, R. (2014). DNA-binding specificities of plant transcription factors and their potential to define target genes. Proc. Natl. Acad. Sci. USA 111, 2367–2372.
- Gupta, S., Stamatoyannopoulos, J.A., Bailey, T.L., and Noble, W.S. (2007). Quantifying similarity between motifs. Genome Biol. 8, R24.
- Schommer, C., Palatnik, J.F., Aggarwal, P., Chételat, A., Cubas, P., Farmer, E.E., Nath, U., and Weigel, D. (2008). Control of jasmonate biosynthesis and senescence by miR319 targets. PLoS Biol. 6, e230.
- Kosugi, S., and Ohashi, Y. (2002). DNA binding and dimerization specificity and potential targets for the TCP protein family. Plant J. 30, 337–348.
- Yin, D., Liu, X., Shi, Z., Li, D., and Zhu, L. (2018). An AT-hook protein DEPRESSED PALEA1 physically interacts with the TCP Family transcription factor RETARDED PALEA1 in rice. Biochem. Biophys. Res. Commun. 495, 487–492.
- Huth, J.R., Bewley, C.A., Nissen, M.S., Evans, J.N., Reeves, R., Gronenborn, A.M., and Clore, G.M. (1997). The solution structure of an HMG-I(Y)-DNA complex defines a new architectural minor groove binding motif. Nat. Struct. Biol. 4, 657–665.
- Solomon, M.J., Strauss, F., and Varshavsky, A. (1986). A mammalian high mobility group protein recognizes any stretch of six A.T base pairs in duplex DNA. Proc. Natl. Acad. Sci. USA 83, 1276–1280.
- Bailey, T.L., and Machanick, P. (2012). Inferring direct DNA binding from ChIP-seq. Nucleic Acids Res. 40, e128.
- Hornitschek, P., Kohnen, M.V., Lorrain, S., Rougemont, J., Ljung, K., López-Vidriero, I., Franco-Zorrilla, J.M., Solano, R., Trevisan, M., Pradervand, S., et al. (2012). Phytochrome interacting factors 4 and 5

- control seedling growth in changing light conditions by directly controlling auxin signaling. Plant J. 71, 699–711.
- 43. Fernández-Calvo, P., Chini, A., Fernández-Barbero, G., Chico, J.M., Gimenez-Ibanez, S., Geerinck, J., Eeckhout, D., Schweizer, F., Godoy, M., Franco-Zorrilla, J.M., et al. (2011). The Arabidopsis bHLH transcription factors MYC3 and MYC4 are targets of JAZ repressors and act additively with MYC2 in the activation of jasmonate responses. Plant Cell 23, 701–715.
- 44. Zhang, Y., Mayba, O., Pfeiffer, A., Shi, H., Tepperman, J.M., Speed, T.P., and Quail, P.H. (2013). A quartet of PIF bHLH factors provides a transcriptionally centered signaling hub that regulates seedling morphogenesis through differential expression-patterning of shared target genes in Arabidopsis. PLoS Genet. 9, e1003244.
- Oh, E., Zhu, J.Y., and Wang, Z.Y. (2012). Interaction between BZR1 and PIF4 integrates brassinosteroid and environmental responses. Nat. Cell Biol. 14, 802–809.
- Kim, D.H., Yamaguchi, S., Lim, S., Oh, E., Park, J., Hanada, A., Kamiya, Y., and Choi, G. (2008). SOMNUS, a CCCH-type zinc finger protein in Arabidopsis, negatively regulates light-dependent seed germination downstream of PIL5. Plant Cell 20, 1260–1277.
- Oh, E., Yamaguchi, S., Hu, J., Yusuke, J., Jung, B., Paik, I., Lee, H.S., Sun, T.P., Kamiya, Y., and Choi, G. (2007). PIL5, a phytochrome-interacting bHLH protein, regulates gibberellin responsiveness by binding directly to the GAI and RGA promoters in Arabidopsis seeds. Plant Cell 19, 1192–1208.
- de Wit, M., Ljung, K., and Fankhauser, C. (2015). Contrasting growth responses in lamina and petiole during neighbor detection depend on differential auxin responsiveness rather than different auxin levels. New Phytol. 208, 198–209.
- Lorrain, S., Allen, T., Duek, P.D., Whitelam, G.C., and Fankhauser, C. (2008). Phytochrome-mediated inhibition of shade avoidance involves degradation of growth-promoting bHLH transcription factors. Plant J. 53, 312–323.
- de Lucas, M., Davière, J.M., Rodríguez-Falcón, M., Pontin, M., Iglesias-Pedraz, J.M., Lorrain, S., Fankhauser, C., Blázquez, M.A., Titarenko, E., and Prat, S. (2008). A molecular framework for light and gibberellin control of cell elongation. Nature 451, 480–484.
- 51. Kunihiro, A., Yamashino, T., Nakamichi, N., Niwa, Y., Nakanishi, H., and Mizuno, T. (2011). Phytochrome-interacting factor 4 and 5 (PIF4 and PIF5) activate the homeobox ATHB2 and auxin-inducible IAA29 genes in the coincidence mechanism underlying photoperiodic control of plant growth of Arabidopsis thaliana. Plant Cell Physiol. 52, 1315–1329.
- 52. Sun, J., Qi, L., Li, Y., Chu, J., and Li, C. (2012). PIF4-mediated activation of YUCCA8 expression integrates temperature into the auxin pathway in regulating arabidopsis hypocotyl growth. PLoS Genet. 8, e1002594.
- Hwang, G., Zhu, J.Y., Lee, Y.K., Kim, S., Nguyen, T.T., Kim, J., and Oh, E. (2017). PIF4 Promotes Expression of *LNG1* and *LNG2* to Induce Thermomorphogenic Growth in *Arabidopsis*. Front. Plant Sci. 8, 1320.
- Peng, M., Li, Z., Zhou, N., Ma, M., Jiang, Y., Dong, A., Shen, W.H., and Li, L. (2018). Linking PHYTOCHROME-INTERACTING FACTOR to histone modification in plant shade avoidance. Plant Physiol. 176, 1341–1351.
- Li, L., Ljung, K., Breton, G., Schmitz, R.J., Pruneda-Paz, J., Cowing-Zitron, C., Cole, B.J., Ivans, L.J., Pedmale, U.V., Jung, H.S., et al. (2012). Linking photoreceptor excitation to changes in plant architecture. Genes Dev. 26, 785–790.
- Nomoto, Y., Kubozono, S., Yamashino, T., Nakamichi, N., and Mizuno, T. (2012). Circadian clock- and PIF4-controlled plant growth: a coincidence mechanism directly integrates a hormone signaling network into the photoperiodic control of plant architectures in Arabidopsis thaliana. Plant Cell Physiol. 53, 1950–1964.
- 57. Gallego-Bartolomé, J., Arana, M.V., Vandenbussche, F., Zádníková, P., Minguet, E.G., Guardiola, V., Van Der Straeten, D., Benkova, E., Alabadí, D., and Blázquez, M.A. (2011). Hierarchy of hormone action controlling apical hook development in Arabidopsis. Plant J. 67, 622–634.

- Sun, J., Qi, L., Li, Y., Zhai, Q., and Li, C. (2013). PIF4 and PIF5 transcription factors link blue light and auxin to regulate the phototropic response in Arabidopsis. Plant Cell 25, 2102–2114.
- Holm, M., Ma, L.G., Qu, L.J., and Deng, X.W. (2002). Two interacting bZIP proteins are direct targets of COP1-mediated control of light-dependent gene expression in Arabidopsis. Genes Dev. 16, 1247–1259.
- 60. Spartz, A.K., Lee, S.H., Wenger, J.P., Gonzalez, N., Itoh, H., Inzé, D., Peer, W.A., Murphy, A.S., Overvoorde, P.J., and Gray, W.M. (2012). The SAUR19 subfamily of SMALL AUXIN UP RNA genes promote cell expansion. Plant J. 70, 978–990.
- 61. Spartz, A.K., Ren, H., Park, M.Y., Grandt, K.N., Lee, S.H., Murphy, A.S., Sussman, M.R., Overvoorde, P.J., and Gray, W.M. (2014). SAUR Inhibition of PP2C-D phosphatases activates plasma membrane H+-ATPases to promote cell expansion in Arabidopsis. Plant Cell 26, 2129–2142.
- Keuskamp, D.H., Pollmann, S., Voesenek, L.A., Peeters, A.J., and Pierik, R. (2010). Auxin transport through PIN-FORMED 3 (PIN3) controls shade avoidance and fitness during competition. Proc. Natl. Acad. Sci. USA 107, 22740–22744.
- 63. Pucciariello, O., Legris, M., Costigliolo Rojas, C., Iglesias, M.J., Hernando, C.E., Dezar, C., Vazquez, M., Yanovsky, M.J., Finlayson, S.A., Prat, S., and Casal, J.J. (2018). Rewiring of auxin signaling under persistent shade. Proc. Natl. Acad. Sci. USA 115, 5612–5617.
- 64. Treml, B.S., Winderl, S., Radykewicz, R., Herz, M., Schweizer, G., Hutzler, P., Glawischnig, E., and Ruiz, R.A. (2005). The gene ENHANCER OF PINOID controls cotyledon development in the Arabidopsis embryo. Development 132, 4063–4074.
- 65. Cheng, Y., Qin, G., Dai, X., and Zhao, Y. (2007). NPY1, a BTB-NPH3-like protein, plays a critical role in auxin-regulated organogenesis in Arabidopsis. Proc. Natl. Acad. Sci. USA 104, 18825–18829.
- 66. Furutani, M., Sakamoto, N., Yoshida, S., Kajiwara, T., Robert, H.S., Friml, J., and Tasaka, M. (2011). Polar-localized NPH3-like proteins regulate polarity and endocytosis of PIN-FORMED auxin efflux carriers. Development 138, 2069–2078.
- 67. Furutani, M., Kajiwara, T., Kato, T., Treml, B.S., Stockum, C., Torres-Ruiz, R.A., and Tasaka, M. (2007). The gene MACCHI-BOU 4/ENHANCER OF PINOID encodes a NPH3-like protein and reveals similarities between organogenesis and phototropism at the molecular level. Development 134, 3849–3859.
- 68. Ranocha, P., Dima, O., Nagy, R., Felten, J., Corratgé-Faillie, C., Novák, O., Morreel, K., Lacombe, B., Martinez, Y., Pfrunder, S., et al. (2013). Arabidopsis WAT1 is a vacuolar auxin transport facilitator required for auxin homoeostasis. Nat. Commun. 4, 2625.
- Steindler, C., Matteucci, A., Sessa, G., Weimar, T., Ohgishi, M., Aoyama, T., Morelli, G., and Ruberti, I. (1999). Shade avoidance responses are mediated by the ATHB-2 HD-zip protein, a negative regulator of gene expression. Development 126, 4235–4245.
- Morelli, G., and Ruberti, I. (1999). Environmental light signals and the development of *Arabidopsis*. In Development, V.E.A. Russo, D.J. Cove, L.G. Edgar, R. Jaenisch, and F. Salamini, eds. (Berlin, Heidelberg: Springer), pp. 199–210.
- Pierik, R., Djakovic-Petrovic, T., Keuskamp, D.H., de Wit, M., and Voesenek, L.A. (2009). Auxin and ethylene regulate elongation responses to neighbor proximity signals independent of gibberellin and della proteins in Arabidopsis. Plant Physiol. 149, 1701–1712.
- Keuskamp, D.H., Sasidharan, R., Vos, I., Peeters, A.J., Voesenek, L.A., and Pierik, R. (2011). Blue-light-mediated shade avoidance requires combined auxin and brassinosteroid action in Arabidopsis seedlings. Plant J. 67, 208–217.
- Wang, Z.Y., Seto, H., Fujioka, S., Yoshida, S., and Chory, J. (2001). BRI1
 is a critical component of a plasma-membrane receptor for plant steroids. Nature 410, 380–383.
- 74. Yamagami, T., Tsuchisaka, A., Yamada, K., Haddon, W.F., Harden, L.A., and Theologis, A. (2003). Biochemical diversity among the 1-amino-

- cyclopropane-1-carboxylate synthase isozymes encoded by the Arabidopsis gene family. J. Biol. Chem. 278, 49102–49112.
- Leivar, P., Monte, E., Al-Sady, B., Carle, C., Storer, A., Alonso, J.M., Ecker, J.R., and Quail, P.H. (2008). The Arabidopsis phytochrome-interacting factor PIF7, together with PIF3 and PIF4, regulates responses to prolonged red light by modulating phyB levels. Plant Cell 20, 337–352.
- Leivar, P., Monte, E., Oka, Y., Liu, T., Carle, C., Castillon, A., Huq, E., and Quail, P.H. (2008). Multiple phytochrome-interacting bHLH transcription factors repress premature seedling photomorphogenesis in darkness. Curr. Biol. 18, 1815–1823.
- Oh, J., Park, E., Song, K., Bae, G., and Choi, G. (2020). PHYTOCHROME INTERACTING FACTOR8 inhibits phytochrome A-mediated far-red light responses in Arabidopsis. Plant Cell 32, 186–205.
- Favero, D.S. (2020). Mechanisms regulating PIF transcription factor activity at the protein level. Physiol. Plant. Published online February 14, 2020. https://doi.org/10.1111/ppl.13075.
- Bernardo-García, S., de Lucas, M., Martínez, C., Espinosa-Ruiz, A., Davière, J.M., and Prat, S. (2014). BR-dependent phosphorylation modulates PIF4 transcriptional activity and shapes diurnal hypocotyl growth. Genes Dev. 28, 1681–1694.
- Ling, J.J., Li, J., Zhu, D., and Deng, X.W. (2017). Noncanonical role of *Arabidopsis* COP1/SPA complex in repressing BIN2-mediated PIF3 phosphorylation and degradation in darkness. Proc. Natl. Acad. Sci. USA 114, 3539–3544.
- 81. Peng, P., Yan, Z., Zhu, Y., and Li, J. (2008). Regulation of the Arabidopsis GSK3-like kinase BRASSINOSTEROID-INSENSITIVE 2 through proteasome-mediated protein degradation. Mol. Plant 1, 338–346.
- 82. Silverstone, A.L., Ciampaglio, C.N., and Sun, T. (1998). The Arabidopsis RGA gene encodes a transcriptional regulator repressing the gibberellin signal transduction pathway. Plant Cell 10, 155–169.
- Dill, A., Jung, H.S., and Sun, T.P. (2001). The DELLA motif is essential for gibberellin-induced degradation of RGA. Proc. Natl. Acad. Sci. USA 98, 14162–14167.
- 84. Silverstone, A.L., Mak, P.Y., Martínez, E.C., and Sun, T.P. (1997). The new RGA locus encodes a negative regulator of gibberellin response in Arabidopsis thaliana. Genetics *146*, 1087–1099.
- 85. Li, K., Yu, R., Fan, L.M., Wei, N., Chen, H., and Deng, X.W. (2016). DELLA-mediated PIF degradation contributes to coordination of light and gibber-ellin signalling in Arabidopsis. Nat. Commun. 7, 11868.
- Feng, S., Martinez, C., Gusmaroli, G., Wang, Y., Zhou, J., Wang, F., Chen, L., Yu, L., Iglesias-Pedraz, J.M., Kircher, S., et al. (2008). Coordinated regulation of Arabidopsis thaliana development by light and gibberellins. Nature 451, 475–479.
- 87. Qiu, Y., Li, M., Kim, R.J.A., Moore, C.M., and Chen, M. (2019). Daytime temperature is sensed by phytochrome B in Arabidopsis through a transcriptional activator HEMERA. Nat. Commun. 10, 140.
- 88. Chen, B., Young, J., and Leng, F. (2010). DNA bending by the mammalian high-mobility group protein AT hook 2. Biochemistry 49, 1590–1595.
- 89. Toledo-Ortiz, G., Johansson, H., Lee, K.P., Bou-Torrent, J., Stewart, K., Steel, G., Rodríguez-Concepción, M., and Halliday, K.J. (2014). The HY5-PIF regulatory module coordinates light and temperature control of photosynthetic gene transcription. PLoS Genet. 10, e1004416.
- Gangappa, S.N., and Kurnar, S.V. (2017). DET1 and HY5 Control PIF4-Mediated Thermosensory Elongation Growth through Distinct Mechanisms. Cell Rep. 18, 344–351.
- 91. Ferrero, L.V., Viola, I.L., Ariel, F.D., and Gonzalez, D.H. (2019). Class I TCP transcription factors target the gibberellin biosynthesis gene GA20ox1 and the growth-promoting genes HBI1 and PRE6 during thermomorphogenic growth in Arabidopsis. Plant Cell Physiol. 60, 1633–1645.
- 92. Han, X., Yu, H., Yuan, R., Yang, Y., An, F., and Qin, G. (2019). Arabidopsis transcription factor TCP5 controls plant thermomorphogenesis by positively regulating PIF4 activity. iScience 15, 611–622.

- Zhou, Y., Xun, Q., Zhang, D., Lv, M., Ou, Y., and Li, J. (2019). TCP transcription factors associate with PHYTOCHROME INTERACTING FACTOR 4 and CRYPTOCHROME 1 to regulate thermomorphogenesis in Arabidopsis thaliana. iScience 15, 600–610.
- Palatnik, J.F., Allen, E., Wu, X., Schommer, C., Schwab, R., Carrington, J.C., and Weigel, D. (2003). Control of leaf morphogenesis by microRNAs. Nature 425, 257–263.
- Martín, G., Rovira, A., Veciana, N., Soy, J., Toledo-Ortiz, G., Gommers, C.M.M., Boix, M., Henriques, R., Minguet, E.G., Alabadí, D., et al. (2018). Circadian waves of transcriptional repression shape PIF-regulated photoperiod-responsive growth in Arabidopsis. Curr. Biol. 28, 311–318.e5.
- Kim, J.H., Lee, H.J., Jung, J.H., Lee, S., and Park, C.M. (2017). HOS1 facilitates the phytochrome B-mediated inhibition of PIF4 function during hypocotyl growth in Arabidopsis. Mol. Plant 10, 274–284.
- Zhu, J.Y., Oh, E., Wang, T., and Wang, Z.Y. (2016). TOC1-PIF4 interaction mediates the circadian gating of thermoresponsive growth in Arabidopsis. Nat. Commun. 7, 13692.
- Pedmale, U.V., Huang, S.C., Zander, M., Cole, B.J., Hetzel, J., Ljung, K., Reis, P.A.B., Sridevi, P., Nito, K., Nery, J.R., et al. (2016). Cryptochromes interact directly with PIFs to control plant growth in limiting blue light. Cell 164, 233–245.
- Nieto, C., López-Salmerón, V., Davière, J.M., and Prat, S. (2015). ELF3-PIF4 interaction regulates plant growth independently of the Evening Complex. Curr. Biol. 25, 187–193.
- 100. Bauer, D., Viczián, A., Kircher, S., Nobis, T., Nitschke, R., Kunkel, T., Panigrahi, K.C., Adám, E., Fejes, E., Schäfer, E., and Nagy, F. (2004). Constitutive photomorphogenesis 1 and multiple photoreceptors control degradation of phytochrome interacting factor 3, a transcription factor required for light signaling in Arabidopsis. Plant Cell 16, 1433–1445.
- Hornitschek, P., Lorrain, S., Zoete, V., Michielin, O., and Fankhauser, C. (2009). Inhibition of the shade avoidance response by formation of non-DNA binding bHLH heterodimers. EMBO J. 28, 3893–3902.
- 102. Ikeda, M., Fujiwara, S., Mitsuda, N., and Ohme-Takagi, M. (2012). A triantagonistic basic helix-loop-helix system regulates cell elongation in Arabidopsis. Plant Cell 24, 4483–4497.
- Hao, Y., Oh, E., Choi, G., Liang, Z., and Wang, Z.Y. (2012). Interactions between HLH and bHLH factors modulate light-regulated plant development. Mol. Plant 5, 688–697.
- 104. Luo, Q., Lian, H.L., He, S.B., Li, L., Jia, K.P., and Yang, H.Q. (2014). COP1 and phyB physically interact with PIL1 to regulate its stability and photomorphogenic development in Arabidopsis. Plant Cell 26, 2441–2456.
- 105. Jégu, T., Veluchamy, A., Ramirez-Prado, J.S., Rizzi-Paillet, C., Perez, M., Lhomme, A., Latrasse, D., Coleno, E., Vicaire, S., Legras, S., et al. (2017). The Arabidopsis SWI/SNF protein BAF60 mediates seedling growth control by modulating DNA accessibility. Genome Biol. 18, 114.
- 106. Campos, M.L., Yoshida, Y., Major, I.T., de Oliveira Ferreira, D., Weraduwage, S.M., Froehlich, J.E., Johnson, B.F., Kramer, D.M., Jander, G., Sharkey, T.D., and Howe, G.A. (2016). Rewiring of jasmonate and phytochrome B signalling uncouples plant growth-defense tradeoffs. Nat. Commun. 7, 12570.
- Langmead, B., Trapnell, C., Pop, M., and Salzberg, S.L. (2009). Ultrafast and memory-efficient alignment of short DNA sequences to the human genome. Genome Biol. 10, R25.
- 108. Robinson, M.D., McCarthy, D.J., and Smyth, G.K. (2010). edgeR: a Bioconductor package for differential expression analysis of digital gene expression data. Bioinformatics 26, 139–140.
- 109. Maere, S., Heymans, K., and Kuiper, M. (2005). BiNGO: a Cytoscape plugin to assess overrepresentation of gene ontology categories in biological networks. Bioinformatics 21, 3448–3449.

- 110. Zhang, Y., Liu, T., Meyer, C.A., Eeckhoute, J., Johnson, D.S., Bernstein, B.E., Nusbaum, C., Myers, R.M., Brown, M., Li, W., and Liu, X.S. (2008). Model-based analysis of ChIP-Seq (MACS). Genome Biol. 9, R137.
- 111. Robinson, J.T., Thorvaldsdóttir, H., Winckler, W., Guttman, M., Lander, E.S., Getz, G., and Mesirov, J.P. (2011). Integrative genomics viewer. Nat. Biotechnol. 29, 24–26.
- 112. Thorvaldsdóttir, H., Robinson, J.T., and Mesirov, J.P. (2013). Integrative Genomics Viewer (IGV): high-performance genomics data visualization and exploration. Brief. Bioinform. 14, 178–192.
- 113. Heinz, S., Benner, C., Spann, N., Bertolino, E., Lin, Y.C., Laslo, P., Cheng, J.X., Murre, C., Singh, H., and Glass, C.K. (2010). Simple combinations of lineage-determining transcription factors prime cis-regulatory elements required for macrophage and B cell identities. Mol. Cell 38, 576–589.
- 114. Ramírez, F., Ryan, D.P., Grüning, B., Bhardwaj, V., Kilpert, F., Richter, A.S., Heyne, S., Dündar, F., and Manke, T. (2016). deepTools2: a next generation web server for deep-sequencing data analysis. Nucleic Acids Res. 44, W160–W165.
- 115. Machanick, P., and Bailey, T.L. (2011). MEME-ChIP: motif analysis of large DNA datasets. Bioinformatics 27, 1696–1697.
- 116. Czechowski, T., Stitt, M., Altmann, T., Udvardi, M.K., and Scheible, W.R. (2005). Genome-wide identification and testing of superior reference genes for transcript normalization in Arabidopsis. Plant Physiol. 139, 5–17.
- 117. Cortijo, S., Charoensawan, V., Brestovitsky, A., Buning, R., Ravarani, C., Rhodes, D., van Noort, J., Jaeger, K.E., and Wigge, P.A. (2017). Transcriptional regulation of the ambient temperature response by H2A.Z nucleosomes and HSF1 transcription factors in Arabidopsis. Mol. Plant 10, 1258–1273.
- 118. Inagaki, S., Takahashi, M., Hosaka, A., Ito, T., Toyoda, A., Fujiyama, A., Tarutani, Y., and Kakutani, T. (2017). Gene-body chromatin modification dynamics mediate epigenome differentiation in *Arabidopsis*. EMBO J. 36. 970–980.
- 119. Rymen, B., Kawamura, A., Lambolez, A., Inagaki, S., Takebayashi, A., Iwase, A., Sakamoto, Y., Sako, K., Favero, D.S., Ikeuchi, M., et al. (2019). Histone acetylation orchestrates wound-induced transcriptional activation and cellular reprogramming in Arabidopsis. Commun Biol 2, 404.
- 120. Seo, P.J., Kim, M.J., Park, J.Y., Kim, S.Y., Jeon, J., Lee, Y.H., Kim, J., and Park, C.M. (2010). Cold activation of a plasma membrane-tethered NAC transcription factor induces a pathogen resistance response in Arabidopsis. Plant J. 61, 661–671.
- Clough, S.J., and Bent, A.F. (1998). Floral dip: a simplified method for Agrobacterium-mediated transformation of Arabidopsis thaliana. Plant J. 16, 735–743.
- 122. Zuo, J., Niu, Q.W., and Chua, N.H. (2000). Technical advance: An estrogen receptor-based transactivator XVE mediates highly inducible gene expression in transgenic plants. Plant J. 24, 265–273.
- 123. Kadota, Y., Macho, A.P., and Zipfel, C. (2016). Immunoprecipitation of plasma membrane receptor-like kinases for identification of phosphorylation sites and associated proteins. Methods Mol. Biol. 1363, 133–144.
- Arabidopsis Interactome Mapping Consortium (2011). Evidence for network evolution in an Arabidopsis interactome map. Science 333, 601–607.
- 125. Chen, D., Xu, G., Tang, W., Jing, Y., Ji, Q., Fei, Z., and Lin, R. (2013). Antagonistic basic helix-loop-helix/bZIP transcription factors form transcriptional modules that integrate light and reactive oxygen species signaling in Arabidopsis. Plant Cell 25, 1657–1673.

STAR***METHODS**

KEY RESOURCES TABLE

REAGENT or RESOURCE	SOURCE	IDENTIFIER
Antibodies		
Anti-GFP antibody - ChIP Grade	Abcam	Cat# ab290; RRID: AB_303395
Anti-Myc tag antibody [9E10] - ChIP Grade	Abcam	Cat# ab32; RRID: AB_303599
Anti-Myc tag antibody [9E10] (HRP)	Abcam	Cat# ab62928; RRID: AB_955371
Anti-Histone H3 antibody - Nuclear Loading Control and ChIP Grade (ab1791)	Abcam	Cat# ab1791; RRID: AB_302613
Chemicals, Peptides, and Recombinant Proteins		
β - Estradiol	Wako Chemicals	CAS 50-28-2
Calcofluor White Stain	Fluka	Cat# 18909
Critical Commercial Assays		
RNeasy Plant Mini Kit	QIAGEN	Cat# 74904
KAPA Stranded mRNA-Seq Kit, with KAPA mRNA Capture Beads	KAPA Biosystems	Cat# KK8420
PrimeScript RT Reagent Kit with gDNA Eraser	Takara Bio	Cat# RR047A
THUNDERBIRD SYBR qPCR Mix	Toyobo	Cat# QPS-101
TruSeq ChIP Library Preparation Kit	Illumina	Cat# IP-202-1024
n-Fusion HD Cloning Kit	Takara Bio	Cat# 639648
Gateway LR Clonase II Enzyme Mix	Thermo Fisher Scientific	Cat# 11791020
Matchmaker Gold Yeast Two-Hybrid System	Takara Bio	Cat# 630489
Gateway BP Clonase II Enzyme Mix	Thermo Fisher Scientific	Cat# 11789020
Qubit dsDNA HS Assay Kit	Thermo Fisher Scientific	Cat# Q32851
Qubit Protein Assay Kit	Thermo Fisher Scientific	Cat #Q33211
Deposited Data		
RNA-seq data	This paper; Gene Expression Omnibus	GEO: GSE122454
SOB3-GFP ChIP-seq data	This paper; Gene Expression Omnibus	GEO: GSE122455
PIF4-myc ChIP-seq data	[45]; Gene Expression Omnibus	GEO: GSE35315
PIF5-myc ChIP-seq data	[42]; Gene Expression Omnibus	GEO: GSE35059
Source data used for figure generation	This paper; Mendeley Data	https://doi.org/10.17632/hp76dxbmwh.1
Experimental Models: Organisms/Strains		
Arabidopsis: WT Col-0	N/A	N/A
Arabidopsis: SOB3-D	[18]	N/A
Arabidopsis: sob3-6	[18]	N/A
Arabidopsis: esc-11	[9]	N/A
Arabidopsis: pif4-101	[49]	GARLIC_114_G06
Arabidopsis: pif4-2	[75]; TAIR	SAIL_1288_E07; CS66043
Arabidopsis: pif4 pif5 pif7	[48]	N/A
Arabidopsis: ProSOB3::SOB3-GFP sob3-4	[16]	N/A
Arabidopsis: pif4-101 sob3-6	This paper	N/A
Arabidopsis: pif4-2 sob3-6	This paper	N/A
Arabidopsis: ProPIF4::PIF4-myc	This paper	N/A
Arabidopsis: ProPIF4::PIF4-myc XVE::SOB3	This paper	N/A
Oligonucleotides		
Primers	See Table S1	N/A
NEBNext Multiplex Oligos for Illumina	New England Biolabs	e.g. Cat# E7335

(Continued on next page)

Continued		
REAGENT or RESOURCE	SOURCE	IDENTIFIER
Recombinant DNA		
pBA-PIF4-6xmyc	This paper	N/A
pER8-GW	This paper	N/A
pER8-GW-SOB3	This paper	N/A
pDONR207-SOB3	This paper	N/A
pDONR207-HY5	This paper	N/A
pENTR223-BZR1	This paper	N/A
pENTR223-PIF4	This paper	N/A
pENTR223-PIF5	This paper	N/A
pGBKT7-SOB3	This paper	N/A
pGADT7-BZR1	This paper	N/A
pGADT7-HY5	This paper	N/A
pGADT7-PIF4	This paper	N/A
pGADT7-PIF5	This paper	N/A
pBTM116-GW-D9-SOB3	[9]	N/A
pACT2-BZR1	This paper	N/A
pACT2-PIF4	This paper	N/A
Software and Algorithms		
Bowtie	[107]	http://bowtie-bio.sourceforge.net/index.shtml
edgeR package in R/Bioconductor	[108]	https://bioconductor.org/packages/release/ bioc/html/edgeR.html
BINGO	[109]	http://apps.cytoscape.org/apps/bingo
MACS2	[110]	https://pypi.org/project/MACS2/
Integrative Genomics Viewer	[111, 112]	https://software.broadinstitute.org/software/igv/
HOMER	[113]	http://homer.ucsd.edu/homer/
deepTools	[114]	https://deeptools.readthedocs.io/en/develop/
MEME-ChIP	[115]	http://meme-suite.org/tools/meme-chip
Real Statistics Resource Pack	N/A	http://www.real-statistics.com/
imageJ	NIH	https://imagej.nih.gov/ij/
Microsoft Excel	Microsoft	N/A
LAS X	Leica	https://www.leica-microsystems.com/products/microscope-software/p/leica-las-x-ls/
Other		
Agencourt AMPure XP	Beckman Coulter	Cat# A63881
Dynabeads Protein A	Thermo Fisher Scientific	Cat# 10002D
Dynabeads Protein G	Thermo Fisher Scientific	Cat# 10003D

LEAD CONTACT AND MATERIALS AVAILABILITY

Further information and requests for resources and reagents should be directed to and will be fulfilled by the Lead Contact, David Favero (david.favero@riken.jp). Plasmids and genetic material generated in this study will be available upon request.

EXPERIMENTAL MODEL AND SUBJECT DETAILS

Plant materials and growth conditions

The wild-type *Arabidopsis thaliana* (L.) accession used in this study was Columbia (Col-0), and all mutants and transgenic lines are in this background. The *pif4-101 sob3-6*, *pif4-2 sob3-6*, *ProPIF4::PIF4-myc*, and *ProPIF4::PIF4-myc XVE::SOB3* lines were generated in this work (see "Preparation of Transgenic Lines and Mutants" below). The *SOB3-D* [18], *sob3-6* [18], *esc-11* [9], *pif4-101* [49], *pif4-2* [75], and *pif4 pif5 pif7* [48] and *ProSOB3::SOB3-GFP sob3-4* [16] lines were all published previously. All lines are homozygous for the specified mutation or transgene.

For most experiments, seeds were surface sterilized and sown on full-strength MS medium containing 0.6% Gelzan CM (Sigma-Aldrich) and no sucrose. 0.8% Gelzan was used instead of 0.6% for ChIP-seq experiments. Seeds were stratified in darkness at 4°C for 2-7 days. Plants for most experiments were grown in MLR-351 plant growth chambers (Sanyo) with a constant temperature of 22°C and a long-day photoperiod (16 h light/8 h darkness). 3LS was used for the light setting, resulting in white fluorescent light with a fluence rate ranging from about 35-55 μ mol/m²/sec. For the experiments testing the effect of SOB3 induction on PIF4 expression and both PIF4-myc binding and protein levels, plants were grown in an LH350-S growth chamber (NK System). Long-day photoperiods were used with 4 as the light setting, resulting in white fluorescent light of about 230-260 μ mol/m²/sec. Temperature was maintained at approximately 22-24°C during the day and night. For these experiments, both ProPIF4::PIF4-myc and ProPIF4::PIF4-myc XVE::SOB3 were grown on regular MS for 13 days and then transferred to medium containing 10 μ M 17 β -estradiol for approximately two days. For mock-treated ProPIF4::PIF4-myc XVE::SOB3 samples, plants were instead transferred to medium containing only the solvent, DMSO.

METHOD DETAILS

Petiole and cell measurements

For petiole length assays, leaf 4 petioles cut from 14 different 21-day-old plants were measured and the four shortest measurements removed, giving n = 10 for each genotype. Petiole length was measured either directly using a digital caliper or on flatbed scanner-generated JPEG format images using ImageJ version 1.51 s (National Institutes of Health, USA). Data were analyzed and graphs generated using Microsoft Excel software. Petiole length assays were performed at least twice and results from one representative experiment shown. For the first experiment measuring cell size only in the middle region of the petiole, images of petiole cortex cells viewed from the abaxial side of the 4th true leaf were captured using bright-field microscopy on a BX53M microscope (Olympus). Using ImageJ, ten consecutive cells in a single longitudinal cell file were measured in the middle region of petioles harvested from ten different plants, giving n = 100 for each genotype. For measurement of cell size along the entire length of petiole, third and fourth true leaves from 3-week-old plants were stained with Calcofluor White Stain (Fluka). An SP8 X confocal laser scanning microscope (Leica) in tile scan mode was used to capture images of abaxial cortex cells along the entire length of the petiole. For each petiole, all cells within one central file of cortex cells were then measured and counted using LAS X software (Leica). For each genotype, six petioles were evaluated and the two with lowest cumulative cell lengths (i.e., the two shortest petioles) removed. Total number of cells measured for each genotype is as follows: WT Col-0, n = 159; sob3-6, n = 202; SOB3-D, n = 97; pif4-101, n = 117.

mRNA extraction

Apical portions of 14- or 15-day-old plants (cut in hypocotyl) were harvested four h after dawn (ZT4) in triplicate (RNA-seq) or quadruplicate (qRT-PCR). Specifically, two to five plants were pooled together to obtain tissue for a single biological replicate with plants for different biological replicates grown on different plates. Samples for different genotypes within the same biological replicate set were harvested from the same plate(s), with an equal number of plants from any given plate used for each genotype. This experimental design was used to minimize the impact of plate-to-plate variation on gene expression. Total RNA was extracted using the RNeasy Plant Mini Kit (QIAGEN) according to manufacturer's instructions, including on-column DNase digestion to eliminate genomic DNA.

RNA sequencing and data analysis

Isolated total RNA was subjected to library preparation using the KAPA Stranded mRNA-Seq Kit (Kapa Biosystems) with NEBNext Multiplex Oligos for Illumina (New England Biolabs) used as adapters and Agencourt AMPure XP (Beckman Coulter) beads used instead of KAPA Pure Beads. Single-end sequencing was performed using the Illumina NextSeq 500 platform. Raw data files (bcl format) were converted to fastq files by bcl2fastq (Illumina). Over 85% of reads were mapped to the *Arabidopsis* TAIR10 cDNA reference using Bowtie 0.12.9 [107] with the following parameters: '-all-best-strata'. The total number of mapped reads per sample was 7-17 million. Differentially expressed transcripts between pairs of samples were identified using the edgeR package in R/Bioconductor [108] with an FDR cutoff of 0.05. AHL-regulated genes were defined as those for which at least one transcript was differentially regulated between *sob3-6* and *SOB3-D*, with any genes excluded for which a transcript was misregulated in the opposite direction between *sob3-6* or *SOB3-D* and the wild-type. PIF-regulated genes were simply defined as those for which at least one transcript was differentially regulated between *pif4 pif5 pif7* and the wild-type. GO enrichment analyses were performed using BINGO [109] in Cytoscape and associated figures generated using Multiple Experiment Viewer software. Venn diagrams were generated using an online tool available at http://bioinformatics.psb.ugent.be/webtools/Venn/. Raw and processed RNA-seq data were deposited into the Gene Expression Omnibus repository (GEO: GSE122454)

Real-time quantitative reverse transcription PCR

Total RNA extracted from apical portions of juvenile rosettes was subjected to first strand cDNA synthesis using the PrimeScript RT Reagent Kit with gDNA Eraser (Takara Bio). Quantitative real-time PCR was performed in duplicate using the THUNDERBIRD SYBR qPCR Mix (Toyobo) with the primers indicated in Table S1. Relative transcript quantities were calculated using standard curves for each primer set and values normalized to the endogenous control, a gene encoding a SERINE/THREONINE PROTEIN PHOSPHATASE 2A (PP2A) subunit (AT1G13320) [116].

Chromatin immunoprecipitation sequencing

Chromatin immunoprecipitation for ChIP-seq was performed in duplicate as described previously with some modifications [117]. About 1 g of whole 14-day-old ProSOB3::SOB3-GFP sob3-4 [16] plants were harvested at ZT4 and immediately frozen using liquid nitrogen. Samples were ground to a fine powder using mortar and pestle and cross-linking performed in 1% formaldehyde for 10 min, after which the nuclear fraction was isolated. Chromatin suspended in nuclei lysis buffer (50 mM Tris-HCl [pH 8], 10 mM EDTA, 1% SDS, 1 Roche cOmplete EDTA-free tablet/50 mL solution) was sheared using a Bioruptor (Diagenode) set to high power with 1.5 mL TPX microtubes (Diagenode) cooled to approximately 4°C. Three sets of seven sonication cycles (30 s on/30 s off) were used, resulting in an average fragment size of approximately 200-400 bp. Sonicated chromatin was immunoprecipitated using an anti-GFP antibody (ab290, Abcam) and Dynabeads Protein A (Thermo Fisher Scientific) at 4°C. Following incubation with antibody, samples were washed twice with low salt wash buffer (20 mM Tris-HCI [pH 8], 150 mM NaCl, 2 mM EDTA, 0.1% SDS, 1% Triton X-100), twice with high salt wash buffer (20 mM Tris-HCl [pH 8], 500 mM NaCl, 2 mM EDTA, 0.1% SDS, 1% Triton X-100), once with LiCl wash buffer (10 mM Tris-HCI [pH 8], 250 mM LiCI, 1% IGEPAL CA-630, 1% sodium deoxycholate, 1 mM EDTA) and twice with TE buffer. Chromatin was eluted from Dynabeads at 65°C in a solution containing 100 mM NaHCO₃, and 1% SDS, and crosslinking was reversed by addition of NaCl to a final concentration of approximately 200 mM. DNA was extracted using Agencourt AMPure XP beads at a 2X ratio. Libraries were constructed from input or ChIPed DNA using the TruSeq ChIP Library Preparation Kit (Illumina) according to manufacturer's instructions, with the exception of the "Purify Ligation Products" step, which was skipped. Library quality was validated using the Agilant 2200 TapeStation with D1000 ScreenTape & Reagents. Qubit dsDNA HS Assay Kit was used with the Qubit 2.0 Fluorometer (Thermo Fisher Scientific) for quantitation of DNA. Single-end sequencing was performed using the Illumina NextSeq 500 platform.

ChIP-seg data analysis

Raw data files (bcl format) for SOB3-GFP generated in this study were converted to fastq files by BaseSpace Sequence Hub (Illumina) or bcl2fastq (Illumina). Over 70% of reads were uniquely mapped to the Arabidopsis TAIR10 reference using Bowtie 0.12.9 [107] with the setting "-m 1." The total number of uniquely mapped reads per sample was 13-16 million. Peaks were called by comparing ChIP samples with the input using the "callpeak" command in MACS2 [110] with the following parameters: "-g 119480000 -m 2 50 -B-SPMR -q 0.05." Fold-enrichment bdg format peak files were generated by using the treatment pileup and control lambda output files generated from "callpeak" as inputs for the MACS2 "bdgcmp" command with the setting "-m FE." Peaks were viewed using Integrative Genomics Viewer (IGV) version 2.3.88 [111, 112]. Visual comparison of peaks revealed similar trends between two SOB3-GFP ChIP replicates. Since the signal to noise ratio was clearly higher for the first replicate, this dataset alone was used for subsequent analyses. Peaks were annotated using HOMER [113]. ChIP-seg and input or mock raw data files (fastg format) for PIF4-myc (GEO: GSE35315) [45], and PIF5-HA (GEO: GSE35059) [42] were obtained from GEO, and processed using the same pipeline as described for SOB3-GFP above. Graphs depicting relative binding of transcription factors in relation to SOB3 peaks summits were generated using the "computeMatrix" and "plotProfile" functions in deepTools [114]. Motif analysis was performed using MEME-ChIP [115] with Arabidopsis PBM motifs selected as known motifs [34]. 300 bp nucleotide sequences centered at the SOB3-GFP ChIP-seq peak summits were used as primary input sequences for MEME-ChIP analysis. Raw and processed ChIP-seq data for SOB3-GFP were deposited into the Gene Expression Omnibus repository (GEO: GSE122455).

ChIP-qPCR

Chromatin immunoprecipitation for ChIP-qPCR was performed as described previously with minor modifications [118, 119]. At least 150 mg of whole 14- or 15-day-old plants were harvested at ZT4 and immediately frozen using liquid nitrogen. Samples were ground to a fine powder using an MB1200 Multi-beads Shocker (Yasui Kikai) and cross-linking performed in 1% formaldehyde for 10 min, after which the nuclear fraction was isolated. Chromatin suspended in SDS lysis buffer (50 mm Tris-HCI [pH 7.8], 1% SDS, 10 mM EDTA) was diluted approximately five-fold with ChIP dilution buffer (50 mm Tris-HCl [pH 7.8], 0.167 M NaCl, 1.1% Triton X-100, 0.11% sodium deoxycholate, 1 Roche cOmplete EDTA-free tablet/50 mL solution) and sheared at 5°C for 15 min using a Covaris S2 Focused-ultrasonicator with milliTUBE 1 mL AFA Fiber tubes (Covaris) and the following settings: duty cycle 5%, intensity 4, and cycles per burst 200. This produced an average fragment size of approximately 100-300 bp. Sonicated chromatin was immunoprecipitated using an anti-myc tag antibody (ab32, Abcam) and Dynabeads Protein G (Thermo Fisher Scientific) at 4°C. Following incubation with antibody, samples were washed once with low salt RIPA buffer (50 mM Tris-HCI [pH 7.8], 150 mM NaCl, 1 mM EDTA, 0.1% SDS, 1% Triton X-100, 0.1% sodium deoxycholate, 1 Roche cOmplete Ultra tablet/50 mL solution), twice with high salt RIPA buffer (50 mM Tris-HCI [pH 7.8], 500 mM NaCl, 1 mM EDTA, 0.1% SDS, 1% Triton X-100, 0.1% sodium deoxycholate, 1 Roche cOmplete Ultra tablet/50 mL solution), once with LNDET (10 mM Tris-HCl [pH 7.8], 250 mM LiCl, 1% IGEPAL CA-630, 1% sodium deoxycholate, 1 mM EDTA) and once with TE buffer. Chromatin was eluted from Dynabeads and cross-linking reversed at 65°C in a solution containing 10 mM Tris-HCI [pH 7.8], 300 mM NaCl, 5 mM EDTA and 0.5% SDS. Phenol-chloroform extraction followed by ethanol precipitation was used to isolate DNA. Quantitative real-time PCR was performed in duplicate for each sample using the THUNDERBIRD SYBR qPCR Mix (Toyobo) with the primers indicated in Table S1. For each of two biologically independent chromatin preps, ChIP was performed in triplicate and results averaged.

Preparation of transgenic lines and mutants

The pif4-101 sob3-6 and pif4-2 sob3-6 double mutants were generated by crossing sob3-6 [18] with pif4-101 (GARLIC_114_G06) [49] and pif4-2 (SAIL_1288_E07) [75], respectively. Double mutants were genotyped using PCR alone, for pif4-101 and pif4-2 alleles, or a cleaved amplified polymorphic sequences (CAPS) marker, in the case of sob3-6 (Table S1). For pif4-101, primers PIF4-LP-1 and PIF4-RP-1 were used to amplify the wild-type PIF4 allele, while PIF4-RP-1 and CSA110-LBs-3 were used for detecting pif4-101 (Table S1). For pif4-2, primers PIF4-LP-2 and PIF4-RP-2 were used to detect PIF4, while PIF4-RP-2 and CSA110-LBs-2 were used to amplify the pif4-2 allele. For sob3-6, SOB3 was amplified using the primers SOB3F+Xhol and SOB3R+Xhol, and the PCR product cut with Fokl, which uniquely cleaves sob3-6, producing fragments of 215 bp and 694 bp. The ProPIF4::PIF4-myc line, which was used in ChIP-qPCR experiments, was constructed by amplifying a 5.8 kb genomic fragment of PIF4 including its promoter, using primers PIF4-F+AvrII and PIF4-R+AscI (Table S1). The PCR product was digested using AvrII and AscI restriction enzymes and then cloned into a modified 6xmyc-pBA vector [120], in which the CaMV 35S promoter was deleted. The resulting binary vector was used for floral dipping [121] of WT Col-0 Arabidopsis. ProPIF4::PIF4-myc transgenic plants were isolated by Basta selection and propagated to obtain homozygous single insertion lines. For generation of the ProPIF4::PIF4-myc XVE::SOB3 line, SOB3 was inserted into a modified pER8 [122] plasmid containing a Gateway cassette (pER8-GW). The pER8-GW plasmid was produced by PCR amplification of a Gateway cassette with primers pER8-Xhol-GW-IF-F and pER8-Spel-GW-IF-R (Table S1) followed by insertion of the product into Xhol/Spel-cut pER8 plasmid using an In-Fusion HD Cloning Kit (Takara Bio). The SOB3 coding sequence was then recombined into pER8-GW from the previously described entry vector pENTR/D-TOPO-SOB3 [18] using Gateway LR Clonase II Enzyme Mix (Thermo Fisher Scientific). The resultant pER8-GW-SOB3 binary vector was used for floral dipping [121] of homozygous ProPIF4::PIF4-myc plants. ProPIF4::PIF4-myc XVE::SOB3 (pER8-GW-SOB3) transgenic plants were isolated by hygromycin selection and propagated to obtain homozygous single insertion lines.

Protein extraction and western blot

Protein isolation and western blotting was performed in triplicate and as previously described [123], with some modifications. 15-day-old whole seedlings were frozen in liquid nitrogen, ground using an MB1200 Multi-beads Shocker (Yasui Kikai), and homogenized in extraction buffer [50mM Tris–HCl pH 7.5, 150 mM NaCl, 10% glycerol, 2mM EDTA, 5 mM DTT, 2% (v/v) IGEPAL CA-630, 2mM Sodium molybdate, 2.5 mM NaF, 1mM PMSF, 1mM Sodium orthovanadate, and 1 Roche cOmplete Ultra tablet/50 mL solution]. After incubation at 4°C for 30 min with gentle rolling, samples were sonicated using a Bioruptor (UCD-250, Cosmo Bio) for 20 s, then incubated at 4°C for another 30 min. PMSF was added to the samples (final concentration of 2.44 mM), which were then centrifuged at 15310 x g at 4°C for 10 min. The supernatant was transferred to a new tube and then centrifuged at 15310 x g at 4°C for 10 min, followed by another centrifugation step (total of 3 centrifugations at 15310 x g at 4°C for 10 min). Protein amount in the final supernatant was quantified using the Qubit Protein Assay Kit with the Qubit 2.0 Fluorometer (Thermo Fisher Scientific) for quantitation of DNA (Thermo Fisher). 15 μ g of protein was then used for SDS-PAGE. Anti-Histone H3 (ab1791, abcam) and anti-myc tag (ab62928, abcam) antibodies were used for detection of proteins.

Yeast two-hybrid

For the data presented in Figures 5A and 5B, the Matchmaker Gold Yeast Two-Hybrid System (Takara Bio) was used according to the manufacturer's instructions. The coding sequences of *SOB3* and *HY5* were amplified by PCR using the primers indicated in Table S1 and cloned into the entry vector pDONR207 using Gateway BP Clonase II Enzyme Mix (Thermo Fisher Scientific). For *BZR1*, *PIF4*, and *PIF5*, the coding sequences were amplified by PCR using the primers indicated in Table S1. The resulting PCR products were cleaved with *Sfi*I and ligated into the pENTR-*Sfi*I-223 vector [124] cut with the same restriction enzyme. All entry vectors were confirmed to be error-free by sequencing. The coding sequence for *SOB3* was then recombined into the bait vector pGBKT7 DNA-BD, while *BZR1*, *HY5*, *PIF4*, or *PIF5* was recombined into the prey vector pGADT7 AD, using Gateway LR Clonase II Enzyme Mix (Thermo Fisher Scientific). The Y2HGold Yeast Strain was sequentially transformed with bait and prey plasmids. Yeast transformants containing both bait and prey were grown on fresh SD medium lacking tryptophan and leucine and then transferred to SD medium without tryptophan, leucine, histidine, and adenine for the binding assay. The binding assay was performed at 30°C for 4 days. PIF3-HYH binding, previously demonstrated to occur in a pull-down assay, was used as a positive control [125].

For the data presented in Figures S5A and S5B, Y2H was performed using a GAL4-based Y2H system, essentially as described previously, with pBTM116-GW-D9-SOB3 as the bait in the L40ccU3 yeast strain [9]. BZR1 or PIF4 in pENTR-Sfil-223 (described above) was recombined into the pACT2-GW prey vector using Gateway LR Clonase II Enzyme Mix (Thermo Fisher Scientific). Yeast transformants containing both bait and prey plasmids were selected on SD medium lacking tryptophan and leucine. For the binding assay, individual colonies were transferred directly to SD medium containing 0.75 mM 3-amino-1, 2, 4-triazol (3-AT) and lacking tryptophan, leucine, histidine, and uracil. Simultaneously, colonies were also plated on SD medium lacking only tryptophan and leucine, in order to verify yeast viability.

QUANTIFICATION AND STATISTICAL ANALYSIS

Where indicated, differences between multiple means were analyzed using one-way analysis of variance (ANOVA) with post hoc Tukey's Honestly Significant Difference (HSD) or Tukey-Kramer test performed with the Real Statistics Resource Pack software (Release 6.6.1; www.real-statistics.com) in Microsoft Excel. The two means in Figure S4B were compared using a two-tailed Welch's



t test. For gene ontology enrichment analysis via BINGO [109], the hypergeometric test was used and the Benjamini and Hochberg False Discovery Rate (FDR) correction applied for calculation of the corrected p values reported in supplemental data files. Significance of overlaps between gene lists generated from RNA-seq and ChIP-seq data were evaluated using the hypergeometric test performed using R version 3.4.1 (www.R-project.org).

DATA AND CODE AVAILABILITY

The RNA-seq and ChIP-seq datasets generated in this study are available on Gene Expression Omnibus: https://www.ncbi.nlm.nih. gov/geo/query/acc.cgi?acc=GSE122456. Other source data used in the preparation of this manuscript, including morphological measurements, average Ct values, and microscopic images are available on Mendeley: https://doi.org/10.17632/hp76dxbmwh.1.